# Adaptive Defense against Harmful Fine-Tuning for Large Language Models via Bayesian Data Scheduler

Zixuan Hu<sup>1</sup> Li Shen<sup>2</sup> Zhenyi Wang<sup>3</sup> Yongxian Wei<sup>4</sup> Dacheng Tao<sup>1\*</sup>

<sup>1</sup>Nanyang Technological University <sup>2</sup>Shenzhen Campus of Sun Yat-sen University

<sup>3</sup> University of Central Florida <sup>4</sup> Tsinghua University

ZIXUAN014@e.ntu.edu.sg mathshenli@gmail.com zhenyi.wang@ucf.edu

weiyx23@mails.tsinghua.edu.cn dacheng.tao@gmail.com

#### **Abstract**

Harmful fine-tuning poses critical safety risks to fine-tuning-as-a-service for large language models. Existing defense strategies preemptively build robustness via attack simulation but suffer from fundamental limitations: (i) the infeasibility of extending attack simulations beyond bounded threat models due to the inherent difficulty of anticipating unknown attacks, and (ii) limited adaptability to varying attack settings, as simulation fails to capture their variability and complexity. To address these challenges, we propose Bayesian Data Scheduler (BDS), an adaptive tuning-stage defense strategy with no need for attack simulation. BDS formulates harmful fine-tuning defense as a Bayesian inference problem, learning the posterior distribution of each data point's safety attribute, conditioned on the fine-tuning and alignment datasets. The fine-tuning process is then constrained by weighting data with their safety attributes sampled from the posterior, thus mitigating the influence of harmful data. By leveraging the post hoc nature of Bayesian inference, the posterior is conditioned on the fine-tuning dataset, enabling BDS to tailor its defense to the specific dataset, thereby achieving adaptive defense. Furthermore, we introduce a neural scheduler based on amortized Bayesian learning, enabling efficient transfer to new data without retraining. Comprehensive results across diverse attack and defense settings demonstrate the state-of-the-art performance of our approach. Code is available at https://github.com/Egg-Hu/Bayesian-Data-Scheduler.

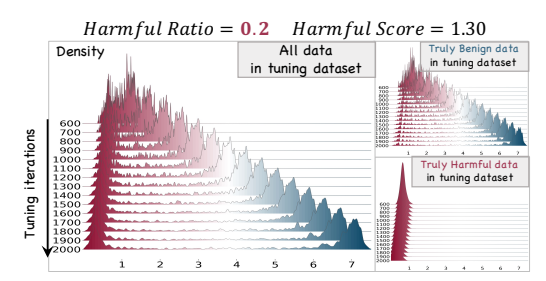
### 1 Introduction

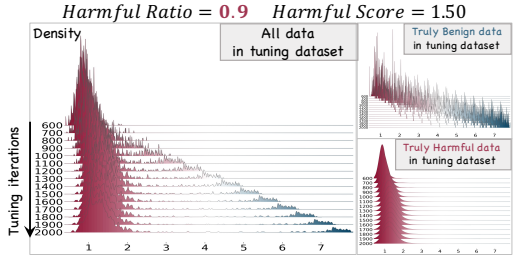
Fine-tuning-as-a-service has become a widely adopted paradigm among mainstream LLM providers (e.g., OpenAI<sup>2</sup>), enabling the delivery of customized language model solutions. In this paradigm, users upload demonstration data representing their desired behaviors, and providers fine-tune the foundational models on their behalf. Despite its growing adoption, recent red teaming studies have uncovered a critical vulnerability: harmful fine-tuning [48, 29]. Harmful fine-tuning refers to that the presence of even a small fraction of harmful data in user-provided datasets can cause fine-tuned models to deviate from the safety alignment established during pre-training. This vulnerability introduces a substantial attack surface and also undermines the reliability and quality of the service.

Existing defenses [29, 33, 52] primarily rely on a *preemptive* manner, aiming to build robustness through attack simulation prior to fine-tuning. However, these defenses suffer from fundamental limitations: (i) the infeasibility of extending attack simulations beyond bounded threat models due to the inherent difficulty of anticipating unknown attacks; and (ii) limited adaptability to varying attack

<sup>\*</sup>Corresponding author: Dacheng Tao

<sup>&</sup>lt;sup>2</sup>Fine-tuning API by OpenAI: https://platform.openai.com/docs/guides/fine-tuning.





Inferred Data Weight (Higher Indicates Greater Likelihood of Being Benign Data)

Figure 1: For encountered datasets with unknown and different harmful ratios, BDS *adaptively* schedules data into higher and lower weight groups during tuning (*largest panels*). To verify correctness of our data scheduling, we observe that most truly benign data indeed receive higher weights (*top right panels*), while almost all truly harmful data consistently receive lower weights (*bottom right panels*).

settings, as the preemptive attack simulation fails to capture the variability and complexity of post hoc attacks. Consequently, their performance deteriorates sharply as the harmful data ratio increases or the attack strategy varies, rendering them ineffective against unpredictable attack surfaces.

To address these challenges, we propose Bayesian Data Scheduler (BDS), an adaptive fine-tuning-stage defense strategy with no need for attack simulation. BDS formulates harmful fine-tuning defense as a Bayesian inference problem, learning the posterior distribution of each data point's safety attribute, conditioned on the fine-tuning and alignment datasets. The fine-tuning is then constrained by weighting data with the safety attributes  $^3$  sampled from the posterior, thus mitigating the negative influence of harmful data. Due to the post hoc nature of Bayesian inference, the posterior is conditioned on the encountered fine-tuning dataset, which enables BDS to precisely tailor its defense to the specific dataset, thus achieving adaptive defense. Additionally, as the posterior of safety attribute is datapoint-wise, *i.e.*,  $p(w_i \mid z_i^{\text{ft}})$ , independently learning distribution for each data point scales with the dataset size and requires relearning for new data. To address scalability and transferability issues, we further introduce a neural scheduler based on amortized Bayesian learning [51], enabling efficient transfer to new data without retraining.

We conduct comprehensive experiments on five diverse downstream datasets using three representative LLM architectures under a wide range of attack and defense settings. Results show that our approach achieves state-of-the-art (SOTA) performance, with a remarkable 74.4% improvement at a high harmful ratio of 0.9 and and an average boost of over 50% across ratios from 0 to 1. Moreover, BDS consistently maintains a remarkably low harmfulness score (around 1) across a wide range of advanced attack dynamics, including benign [48], out-of-distribution (OOD), and identity-shifting [48] attacks, demonstrating superior effectiveness, adaptiveness, and robustness.

To the end, we summarize our contributions as follows:

- For the first time, we formulate harmful fine-tuning defense as a Bayesian inference problem, offering a principled framework BDS achieving adaptive defense with no need for attack simulation.
- We propose two BDS implementations, with the neural version enabling efficient transfer to new
  data without retraining. Leveraging post hoc nature of Bayesian inference, BDS learns the posterior
  distribution of data weights conditioned on specific datasets, thus achieving adaptive defense.
- Comprehensive experiments on diverse attack and defense settings demonstrate the SOTA performance and superior adaptiveness of our proposed method.

#### 2 Problem Definition

**Scenario.** The scenario considers users uploading a personalized fine-tuning dataset  $\mathcal{D}_{ft}$ , which the service provider uses to fine-tune their model  $\theta$ . Once fine-tuned, the personalized API is returned for user-specific applications.

**Threat model.** Harmful fine-tuning arises when an attacker deliberately uploads a fine-tuning dataset  $\mathcal{D}_{\mathrm{ft}}$  that contains a mix of benign and harmful data. Specifically, the dataset  $\mathcal{D}_{\mathrm{ft}}$  consists

<sup>&</sup>lt;sup>3</sup>In this paper, "safety attribute" and "data weight" are used synonymously.

of a proportion p of harmful data and 1-p of benign data, such that  $\mathcal{D}_{\mathrm{ft}} = \mathcal{D}_{\mathrm{ft}}^{\mathrm{benign}} \cup \mathcal{D}_{\mathrm{ft}}^{\mathrm{harmful}}$ . The attacker, acting as a user, has the capacity to control the composition of the fine-tuning dataset, including the proportion and content of harmful data, without requiring knowledge of the model's architecture or parameters. On the other hand, the defender, acting as the service provider, has the capacity to control the fine-tuning process.

**Assumption.** We assume that the service provider maintains an alignment dataset, denoted as  $\mathcal{D}_{\text{safe}}$  (harmful prompt-safe answer pairs). The availability of such an alignment dataset has been previously discussed in previous works [52, 57] and it is available in publicly available resources (*e.g.*, BeaverTail [35]). While prior studies require an additional harmful dataset for attack simulation, constructing such a dataset is difficult due to lacking prior knowledge about unknown and varying attack data  $\mathcal{D}_{\text{fr}}^{\text{harmful}}$ . Our work overcomes this limitation with no need for a simulated harmful dataset.

## 3 Related work.

Mechanism study of harmful fine-tuning. Recent works have investigated why LLMs are highly sensitive to harmful fine-tuning. (i) Adversarial perturbations: Harmful fine-tuning can introduce adversarial shifts in model parameters [29, 46] or embeddings [33], leading to degraded safety alignment. (ii) Structural vulnerabilities: Other works highlight that certain layers or modules are more critical for maintaining safety than others [21, 37, 47]. (iii) *Catastrophic forgetting:* Safety alignment degradation has also been linked to *catastrophic forgetting* [43], where alignment knowledge tends to be lost under the sequential training paradigm [6, 13].

**Harmful fine-tuning attack.** On the attack side, [48] demonstrate that even fine-tuning solely on benign data can inadvertently weaken a model's safety alignment. Subsequent work [20] further identifies specific subsets of benign data that are particularly prone to degrading model safety after fine-tuning. [18] introduce covert malicious fine-tuning, which enhances the stealthiness of such attacks, while [32] construct harmful data designed to deliberately circumvent moderation guardrails.

Harmful fine-tuning defense. On the defense side, existing defense methods can be categorized into three main categories, including alignment stage [33, 52, 58, 42, 29, 40, 41, 7, 75], fine-tuning stage [44, 3, 31, 61, 79, 55], and post-fine-tuning stage solutions [76, 12, 28, 70, 62]. The method proposed in this paper should be classified into a fine-tuning stage solution. However, it differs fundamentally from prior work in that we propose a loss-based data scheduling mechanism derived from Bayesian inference principles, whereas previous approaches typically perform hard-label data selection based on less effective heuristic rules [15, 5] or manually tuned thresholds [8, 55]. Moreover, unlike the current SOTA method Booster [29], our method does not require attack simulation, making it more practical and efficient while achieving strong defense performance and adaptability.

A more detailed and extended review of related work is provided in App. A.

## 4 Methodology

In this section, we introduce the Bayesian Data Scheduler method. Specifically, we outline our framework in Sec. 4.1. Following that, we detail two implementations of BDS, including Bayesian Scalar Scheduler and Amortized Bayesian Neural Scheduler in Secs. 4.2 and 4.3.

## 4.1 Bayesian Data Scheduler Framework

We frame the harmful fine-tuning defense as a Bayesian inference framework, with its underlying graphical model depicted in Fig. 2. For clarity, the discussion here focuses on the left panel, with the right panel deferred to Sec. 4.3. Each data point  $\boldsymbol{z}_i^{\text{ft}}$  in the fine-tuning dataset  $\mathcal{D}_{\text{ft}}$  is associated with another latent variable  $w_i \in \mathbb{R}$ , indicating its intrinsic safety attribute (i.e.,  $\boldsymbol{z}_i^{\text{ft}} \to w_i$ ). To mitigate the negative effect of potentially harmful data, the fine-tuning process  $(w_i, \boldsymbol{z}_i^{\text{ft}}) \to \boldsymbol{\theta}$  is constrained, where the contribution of each data point  $\boldsymbol{z}_i^{\text{ft}}$  to update the model  $\boldsymbol{\theta}$ 

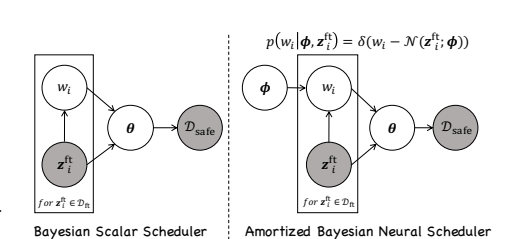


Figure 2: Graphical models for the Bayesian Scalar Scheduler (see Sec. 4.2) and Amortized Bayesian Neural Scheduler (see Sec. 4.3).

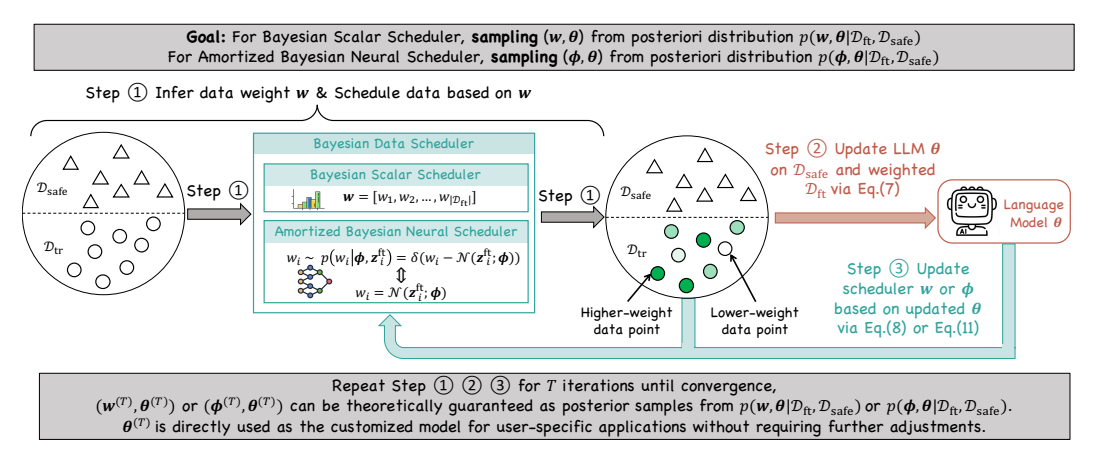


Figure 3: Pipeline of BDS. *Step 1:* BDS first infer the weight of each data point, indicating its safety attribute. *Step 2:* BDS updates the LLM  $\theta$  with weighted data via Eq. (7). *Step 3:* BDS update the scheduler w or  $\phi$  via Eq. (8) or Eq. (11). Repeat steps 1-3 for T iterations until convergence and  $(w^{(T)}, \theta^{(T)})$  or  $(\phi^{(T)}, \theta^{(T)})$  can be theoretically guaranteed as posterior samples.  $\theta^{(T)}$  is directly used as the customized model for user-specific applications without requiring further adjustments. For clarity, the pseudocode for the BDS algorithm is provided in App. C.

is modulated by its safety attribute  $w_i$ . The edge  $\theta \to \mathcal{D}_{safe}$  represents the generation of the target parts of the alignment dataset  $\mathcal{D}_{safe}$ , modeling the likelihood of observing  $\mathcal{D}_{safe}$  given  $\theta$ . The data points are assumed to be i.i.d., implying that  $p(\boldsymbol{w}) = \prod_i p(w_i)$  holds, where  $w_i$  is the i-th component of vector  $\boldsymbol{w}$ . The conditional independence  $\mathcal{D}_{safe} \perp (\boldsymbol{w}, \mathcal{D}_{ft}) \mid \boldsymbol{\theta}$  naturally holds from the structure of the graphical model.

**Goal.** Our goal is to infer the posterior distributions of unobserved variables (unshaded nodes): *i.e.*, the data weights  $\boldsymbol{w}$  and the model parameters  $\boldsymbol{\theta}$ , conditioned on observed variables (shaded nodes), *i.e.*, the safety alignment dataset  $\mathcal{D}_{\text{safe}}$  and the fine-tuning dataset  $\mathcal{D}_{\text{ft}}$ . Formally, this corresponds to estimating the joint posterior:  $p(\boldsymbol{w}, \boldsymbol{\theta} \mid \mathcal{D}_{\text{ft}}, \mathcal{D}_{\text{safe}})$ .

# 4.2 Bayesian Scalar Scheduler

**Posterior decomposition.** To address the computational intractability of directly inferring the posterior distribution  $p(\mathbf{w}, \boldsymbol{\theta} \mid \mathcal{D}_{\text{ft}}, \mathcal{D}_{\text{safe}})$ , we decompose it as follows:

$$p(\boldsymbol{\theta}, \boldsymbol{w} \mid \mathcal{D}_{\text{ft}}, \mathcal{D}_{\text{safe}}) \propto p(\mathcal{D}_{\text{safe}} \mid \boldsymbol{\theta}) \cdot p(\mathcal{D}_{\text{ft}} \mid \boldsymbol{\theta}, \boldsymbol{w}) \cdot p(\mathcal{D}_{\text{ft}} \mid \boldsymbol{w})^{-1} \cdot p(\boldsymbol{\theta}, \boldsymbol{w}).$$
 (1)

Detailed derivations are provided in App. H.1. The term  $p(\mathcal{D}_{safe} \mid \boldsymbol{\theta})$  in Eq. (1) represents the likelihood of observing the alignment dataset  $\mathcal{D}_{safe}$  given the model parameters  $\boldsymbol{\theta}$ , quantifying how well the model aligns with the alignment dataset. Based on the conventional trick [82], this likelihood can be formulated in terms of the loss function as follows:

$$p\left(\mathcal{D}_{\mathrm{safe}} \mid \boldsymbol{\theta}\right) \propto \prod_{i=1}^{|\mathcal{D}_{\mathrm{safe}}|} \exp\left(-\ell\left(\boldsymbol{z}_{i}^{\mathrm{safe}}; \boldsymbol{\theta}\right)\right),$$
 (2)

where  $|\mathcal{D}_{\text{safe}}|$  denotes the size of the dataset and  $\ell(\cdot)$  denotes the loss function. Next, the second term  $p(\mathcal{D}_{\text{ft}} \mid \boldsymbol{\theta}, \boldsymbol{w})$  in Eq. (1) represents the likelihood of the fine-tuning dataset  $\mathcal{D}_{\text{ft}}$  given the model parameters  $\boldsymbol{\theta}$  and the safety attributes  $\boldsymbol{w}$ , where the contribution of each data point  $\boldsymbol{z}_i^{\text{ft}}$  is modulated by its safety weight  $w_i$ :

$$p(\mathcal{D}_{\mathrm{ft}} \mid \boldsymbol{\theta}, \boldsymbol{w}) \propto \prod_{i=1}^{|\mathcal{D}_{\mathrm{ft}}|} \exp\left(-\sigma(w_i) \cdot \ell\left(\boldsymbol{z}_i^{\mathrm{ft}}; \boldsymbol{\theta}\right)\right),$$
 (3)

where  $\sigma(\cdot)$  refers to the weight transformation function, which is discussed in detail in Sec. 4.4.

The term  $p\left(\mathcal{D}_{\mathrm{ft}} \mid \boldsymbol{w}\right)^{-1}$  in Eq. (1) represents the likelihood of the fine-tuning dataset  $\mathcal{D}_{\mathrm{ft}}$  given the safety attributes  $\boldsymbol{w}$ . Since it is infeasible to directly model the relationship  $\mathcal{D}_{\mathrm{ft}} \to \boldsymbol{w}$ , we employ

marginalization over  $\theta$  and approximate it using the maximum a posteriori (MAP) estimate (Detailed derivations are provided in App. H.2.):

$$p\left(\mathcal{D}_{\mathrm{ft}} \mid \boldsymbol{w}\right)^{-1} \propto \prod_{i=1}^{|\mathcal{D}_{\mathrm{ft}}|} \exp\left(\sigma(w_{i}) \cdot \ell\left(\boldsymbol{z}_{i}^{\mathrm{ft}}; \hat{\boldsymbol{\theta}}\right)\right), \quad \text{s.t.,} \quad \hat{\boldsymbol{\theta}} = \arg\max_{\boldsymbol{\theta}} \mathbb{E}_{p\left(\mathcal{D}_{\mathrm{ft}} \mid \boldsymbol{w}\right)} \left[\left(p\left(\boldsymbol{\theta} \mid \mathcal{D}_{\mathrm{ft}}, \boldsymbol{w}\right)\right)\right]. \tag{4}$$

Efficient Posterior inference via Stochastic Gradient Langevin Dynamic (SGLD) sampling. Due to the intractability of obtaining closed-form solutions for Eq. (1), we employ an efficient posterior inference technique based on stochastic-gradient Markov Chain Monte Carlo (SG-MCMC) [45]. Specifically, we utilize Stochastic Gradient Langevin Dynamics (SGLD) [69] to sample from the posterior  $p(w, \theta \mid \mathcal{D}_{\rm ft}, \mathcal{D}_{\rm safe})$ , inspired by [49, 17, 73, 10]. By iteratively updating the system under the Langevin dynamics framework, we can obtain theoretically guaranteed posterior samples once the process converges (convergence analysis is provided in App. G.2).

$$[\boldsymbol{\theta}, \boldsymbol{w}] \leftarrow [\boldsymbol{\theta}, \boldsymbol{w}] + \frac{\eta}{2} \nabla_{\boldsymbol{\theta}, \boldsymbol{w}} \log p(\boldsymbol{\theta}, \boldsymbol{w} \mid \mathcal{D}_{\text{ft}}, \mathcal{D}_{\text{safe}}) + \epsilon \sqrt{\eta},$$
 (5)

where  $\eta$  represents the step size, and  $\epsilon \sim \mathcal{G}(0,I)$  denotes Gaussian noise introduced to inject randomness. Based on the posterior decomposition in Eq. (1), the gradient of the log-posterior can be expressed as a summation:

$$\nabla_{\boldsymbol{\theta}, \boldsymbol{w}} \log p\left(\boldsymbol{\theta}, \boldsymbol{w} \mid \mathcal{D}_{\text{ft}}, \mathcal{D}_{\text{safe}}\right) = \nabla_{\boldsymbol{\theta}, \underline{-}} \log p(\mathcal{D}_{\text{safe}} \mid \boldsymbol{\theta}) + \nabla_{\boldsymbol{\theta}, \boldsymbol{w}} \log p(\mathcal{D}_{\text{ft}} \mid \boldsymbol{\theta}, \boldsymbol{w}) + \nabla_{\boldsymbol{\theta}, \boldsymbol{w}} \log p(\mathcal{D}_{\text{ft}} \mid \boldsymbol{w})^{-1} + \nabla_{\boldsymbol{\theta}, \boldsymbol{w}} \log p(\boldsymbol{\theta}, \boldsymbol{w}),$$
(6)

where placeholder \_ denotes independence between the gradient term and the corresponding variable. To improve the efficiency of gradient computation, SGLD substitutes the full-batch likelihood in with a minibatch approximation. Using minibatch  $\mathcal{B}$ , we reformulate Eq. (6) using the decompositions in Eqs. (2) to (4), yielding the following equations.

$$\boldsymbol{\theta} \leftarrow \boldsymbol{\theta} + \frac{\eta}{2} \nabla_{\boldsymbol{\theta}} \left( \log p(\boldsymbol{\theta} \mid \boldsymbol{w}) - \frac{|\mathcal{D}_{\text{safe}}|}{|\mathcal{B}_{\text{safe}}|} \sum_{\boldsymbol{z}_{i}^{\text{safe}} \in \mathcal{B}_{\text{safe}}} \ell(\boldsymbol{z}_{i}^{\text{safe}}; \boldsymbol{\theta}) - \frac{|\mathcal{D}_{\text{ft}}|}{|\mathcal{B}_{\text{ft}}|} \sum_{\boldsymbol{z}_{i}^{\text{ft}} \in \mathcal{B}_{\text{ft}}} \left[ \sigma(w_{i}) \cdot \ell(\boldsymbol{z}_{i}^{\text{ft}}; \boldsymbol{\theta}) \right] \right) + \epsilon \sqrt{\eta},$$
(7)

$$w \leftarrow w + \frac{\eta}{2} \nabla_{w} \left( \log p(w) - \frac{|\mathcal{D}_{\text{ft}}|}{|\mathcal{B}_{\text{ft}}|} \sum_{\boldsymbol{z}_{i}^{\text{ft}} \in \mathcal{B}_{\text{ft}}} \left[ \sigma(w_{i}) \cdot (\ell(\boldsymbol{z}_{i}^{\text{ft}}; \boldsymbol{\theta}) - \ell(\boldsymbol{z}_{i}^{\text{ft}}; \hat{\boldsymbol{\theta}})) \right] \right) + \epsilon \sqrt{\eta}$$

$$\approx w + \frac{\eta}{2} \nabla_{w} \left( \log p(w) - \frac{|\mathcal{D}_{\text{ft}}|}{|\mathcal{B}_{\text{ft}}|} \sum_{\boldsymbol{z}_{i}^{\text{ft}} \in \mathcal{B}_{\text{ft}}} \left[ \sigma(w_{i}) \cdot \ell(\boldsymbol{z}_{i}^{\text{ft}}; \boldsymbol{\theta}) \right] \right) + \epsilon \sqrt{\eta},$$
(8)

where we approximate  $\ell(\boldsymbol{z}_i^{\mathrm{ft}}; \hat{\boldsymbol{\theta}}) \approx 0$ . This is justified as  $\hat{\boldsymbol{\theta}} = \arg \max_{\boldsymbol{\theta}} \mathbb{E}_{p(\mathcal{D}_{\mathrm{ft}}|\boldsymbol{w})} \left[ (p(\boldsymbol{\theta} \mid \mathcal{D}_{\mathrm{ft}}, \boldsymbol{w})) \right]$  (see Eq. (4)), which represents the MAP estimate of the model  $\boldsymbol{\theta}$  given the dataset  $\mathcal{D}_{\mathrm{ft}}$ . Intuitively,  $\hat{\boldsymbol{\theta}}$  is optimized to perform well on  $\mathcal{D}_{\mathrm{ft}}$ , resulting in a near-zero loss.

Intuition behind weight update in Eq. (8) (see Fig. 4). By omitting the prior term, noise, and constants, the update of the i-th component of  $\boldsymbol{w}$  in the non-approximated Eq. (8) simplifies to:  $w_i \leftarrow w_i - \left(\ell(\boldsymbol{z}_i^{\text{ft}}; \boldsymbol{\theta}) - \ell(\boldsymbol{z}_i^{\text{ft}}; \hat{\boldsymbol{\theta}})\right) \cdot \nabla_{w_i} \sigma(w_i)$ . In this form, the loss gap scales the gradient term  $\nabla_{w_i} \sigma(w_i)$ , where a larger loss gap leads to a significant reduction in  $w_i$ , ultimately resulting in a smaller weight. Within the loss gap,  $\boldsymbol{\theta}$  is derived via Eq. (7), which optimizes over both  $\mathcal{D}_{\text{safe}}$  and the weighted  $\mathcal{D}_{\text{ft}}$ , thus referred to as the safety-aware model. In contrast,  $\hat{\boldsymbol{\theta}}$  is obtained through Eq. (4), fitting only the weighted  $\mathcal{D}_{\text{ft}}$ , thus re-

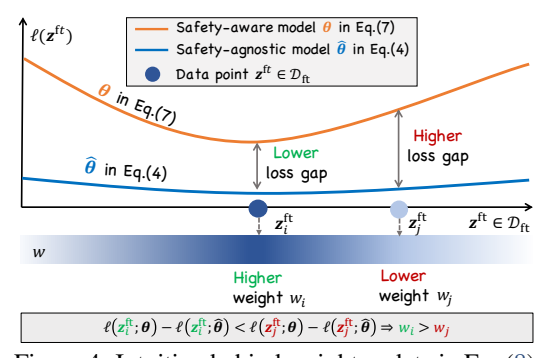


Figure 4: Intuition behind weight update in Eq. (8).

ferred to as the safety-agnostic model. If a data point  $z_i^{\rm ft}$  produces a large positive loss gap, it indicates poorer alignment with the safety-aware model  $\theta$  compared to the safety-agnostic model  $\hat{\theta}$ . This suggests that  $z_i^{\rm ft}$  is likely misaligned with the safe dataset  $\mathcal{D}_{\rm safe}$ , ultimately resulting in a larger weight reduction, and thus a smaller assigned weight.

#### 4.3 Amortized Bayesian Neural Scheduler

The Bayesian Scalar Scheduler introduced in Sec. 4.2 provides a strong foundation but leaves room for further enhancement in two key aspects: (i) Scalability: Inferring  $w_i \sim p(w_i \mid \boldsymbol{z}_i^{\text{ft}}, \mathcal{D}_{\text{safe}})$  for each data point scales with dataset size. (ii) Transferability: Without explicitly modeling  $\boldsymbol{z}_i^{\text{ft}} \to w_i$ , posterior inference must restart from scratch when new data is added.

To address the scalability and transferability issues, we introduce the Amortized Bayesian Neural Scheduler based on amortized Bayesian learning [51]. The core idea is to amortize the effort for inferring datapoint-wise posterior  $p(w_i \mid \boldsymbol{z}_i^{\rm ft}, \mathcal{D}_{\rm safe})$  into inferring just one posterior of a neural network  $p(\phi \mid \mathcal{D}_{\rm ft}, \mathcal{D}_{\rm safe})$ . As shown in the right panel of Fig. 2, the neural network  $\phi \sim p(\phi \mid \mathcal{D}_{\rm ft}, \mathcal{D}_{\rm safe})$  is shared across all data points, enabling each  $p(w_i \mid \boldsymbol{z}_i^{\rm ft}, \mathcal{D}_{\rm safe})$  to be inferred efficiently via a forward pass through the network conditioned on  $\boldsymbol{z}_i^{\rm ft}$ . For simplicity, we define  $p(w_i \mid \boldsymbol{z}_i^{\rm ft}, \mathcal{D}_{\rm safe})$  as a Dirac delta distribution  $\delta(\cdot)$ , whose single value is determined by the output of a neural network  $\mathcal{N}(\boldsymbol{z}_i^{\rm ft} \mid \phi)$  with  $\boldsymbol{z}_i^{\rm ft}$  as input. After introducing  $\phi$ , the datapoint-wise posterior is expressed as:

$$p(w_i \mid \boldsymbol{\phi}, \boldsymbol{z}_i^{\text{ft}}) := \delta\left(w_i - \mathcal{N}(\boldsymbol{z}_i^{\text{ft}} \mid \boldsymbol{\phi})\right).$$
 (9)

In this way, only a single posterior over the neural network parameters (i.e.,  $p(\phi \mid \mathcal{D}_{\mathrm{ft}}, \mathcal{D}_{\mathrm{safe}})$ ) needs to be inferred, and the posterior of weights for new data can be inferred seamlessly through forward passes without retraining.

After introducing  $\phi$ , the updated probabilistic graphical model is illustrated in the right panel of Fig. 2. Consequently, our inference objective shifts from  $p(\boldsymbol{w}, \boldsymbol{\theta} \mid \mathcal{D}_{\mathrm{ft}}, \mathcal{D}_{\mathrm{safe}})$  to  $p(\phi, \boldsymbol{\theta} \mid \mathcal{D}_{\mathrm{ft}}, \mathcal{D}_{\mathrm{safe}})$ , which can be decomposed as follows (Detailed proof is provided in App. H.3):

$$p(\boldsymbol{\theta}, \boldsymbol{\phi} \mid \mathcal{D}_{\text{ft}}, \mathcal{D}_{\text{safe}}) \propto p(\mathcal{D}_{\text{safe}} \mid \boldsymbol{\theta}) \cdot p(\mathcal{D}_{\text{ft}} \mid \boldsymbol{\theta}, \boldsymbol{w}) \cdot p(\mathcal{D}_{\text{ft}} \mid \boldsymbol{w})^{-1} \cdot p(\boldsymbol{\theta}, \boldsymbol{\phi} \mid \mathcal{D}_{\text{ft}}),$$
s.t., 
$$\boldsymbol{w} = \mathcal{N}(\mathcal{D}_{\text{ft}} \mid \boldsymbol{\phi}) \triangleq \left[ \mathcal{N}(\boldsymbol{z}_{1}^{\text{ft}} \mid \boldsymbol{\phi}), \cdots, \mathcal{N}(\boldsymbol{z}_{|\mathcal{D}_{\text{ft}}|}^{\text{ft}} \mid \boldsymbol{\phi}) \right].$$
(10)

Similar to Eq. (8), we derive the update rule for  $\phi$ :

$$\phi \leftarrow \phi + \frac{\eta}{2} \nabla_{\phi} \left( \log p(\phi) - \frac{|\mathcal{D}_{\text{ft}}|}{|\mathcal{B}_{\text{ft}}|} \sum_{\boldsymbol{z}_{i}^{\text{ft}} \in \mathcal{B}_{\text{ft}}} \left[ \sigma(\mathcal{N}(\boldsymbol{z}_{i}^{\text{ft}}; \phi)) \cdot \ell(\boldsymbol{z}_{i}^{\text{ft}}; \boldsymbol{\theta}) \right] \right) + \epsilon \sqrt{\eta}.$$
(11)

## 4.4 Data Weight Transformation

Recall the scheduler updates in Eqs. (8) and (11). We identify a key factor that significantly impacts the performance of BDS: the weight transformation function  $\sigma(w_i)$ . As shown in Fig. 5, different transformation functions result in varying sampling trajectories of  $\boldsymbol{w}$  for benign and harmful data, ultimately leading to distinct defensive capabilities (see Tab. 14). For clarity, we first introduce the definition of the SGLD Sampling Trajectory:

**Definition 4.1.** (SGLD Sampling Trajectory) The SGLD Sampling Trajectory refers to the sequence of states generated during the iterative sampling process of SGLD. This sequence forms a Markov chain, where each state transition depends solely on the previous state. For the distribution  $p(\boldsymbol{w}, \boldsymbol{\theta} \mid \mathcal{D}_{\mathrm{ft}}, \mathcal{D}_{\mathrm{safe}})$ , the trajectories of the variables  $\boldsymbol{w}$  and  $\boldsymbol{\theta}$  can be defined as:

$$\operatorname{Tr}_{\boldsymbol{w}} = \boldsymbol{w}^{(0)} \to \cdots \to \boldsymbol{w}^{(T)}, \ \boldsymbol{w}^{(t+1)} = \boldsymbol{w}^{(t)} + \frac{\eta}{2} \nabla_{\boldsymbol{w}}^{(t)} + \epsilon \sqrt{\eta},$$

$$\operatorname{Tr}_{\boldsymbol{\theta}} = \boldsymbol{\theta}^{(0)} \to \cdots \to \boldsymbol{\theta}^{(T)}, \ \boldsymbol{\theta}^{(t+1)} = \boldsymbol{\theta}^{(t)} + \frac{\eta}{2} \nabla_{\boldsymbol{\theta}}^{(t)} + \epsilon \sqrt{\eta}.$$
(12)

Here, we use  $\nabla_{w}$  and  $\nabla_{\theta}$  to denote the gradient terms in Eqs. (7) and (8). We next analyze the effect of different transformation functions on the term  $\nabla_{w}$  in Eq. (12).

We consider three types of weight transformations: *identity*, *sigmoid*, and *softmax*, which are formally defined as:

$$\sigma(w_i) = w_i \quad (identity), \quad \bar{\sigma}(w_i) = \frac{1}{1 + \exp(-w_i)} \quad (sigmoid),$$

$$\bar{\bar{\sigma}}(w_i) = \frac{\exp(w_i)}{\sum_{j=1}^{|\mathcal{D}_{\text{ft}}|} \exp(w_j)} \quad (softmax).$$
(13)

By differentiating w in Eq. (8) (excluding prior and constant coefficients), we derive that under the identity transformation, w updates in a monotonically decreasing manner:

$$\nabla_{w_i} = -\ell\left(\boldsymbol{z}_i^{\text{ft}}; \boldsymbol{\theta}\right) < 0. \tag{14}$$

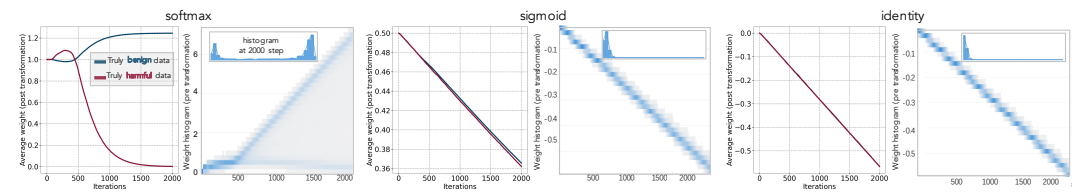


Figure 5: Effect of weight transformation on SGLD sampling trajectories of w for benign and harmful data, respectively. For clarity, weights post-softmax are scaled by  $|\mathcal{D}_{\text{safe}}|$ .

Similarly, under sigmoid, the weight w also exhibits a monotonically decreasing update behavior:

$$\nabla_{w_i} = -\bar{\sigma}(x) \cdot (1 - \bar{\sigma}(x)) \cdot \ell\left(\boldsymbol{z}_i^{\text{ft}}; \boldsymbol{\theta}\right) < 0.$$
 (15)

Since the gradient of  $\boldsymbol{w}$  is proportional to the negative loss, the weight suboptimality under both identity and sigmoid transformation primarily arises from the uniform treatment of benign and harmful data, resulting in monotonically decreasing weights for both. As demonstrated in Fig. 5, this causes the scheduler to assign reduced weights to both benign and harmful data to preserve the model's inherent safety alignment, which is equivalent to discarding any data and consequently leads to poor fine-tuning performance.

In contrast, under softmax, the weight w updates in an adaptively bidirectional manner:

$$\nabla_{w_i} = -\bar{\bar{\sigma}}(w_i) \cdot \left(\ell(\boldsymbol{z}_i^{\mathrm{f}}; \boldsymbol{\theta}) - \sum_{k=1}^{|\mathcal{D}_{\mathrm{fi}}|} \bar{\bar{\sigma}}(w_k) \cdot \ell(\boldsymbol{z}_k^{\mathrm{f}}; \boldsymbol{\theta})\right) \begin{cases} > 0, & \text{if } \ell(\boldsymbol{z}_i^{\mathrm{f}}; \boldsymbol{\theta}) < \sum_{k=1}^{|\mathcal{D}_{\mathrm{fi}}|} \bar{\bar{\sigma}}(w_k) \cdot \ell(\boldsymbol{z}_k^{\mathrm{fi}}; \boldsymbol{\theta}) \\ < 0, & \text{if } \ell(\boldsymbol{z}_i^{\mathrm{fi}}; \boldsymbol{\theta}) > \sum_{k=1}^{|\mathcal{D}_{\mathrm{fi}}|} \bar{\bar{\sigma}}(w_k) \cdot \ell(\boldsymbol{z}_k^{\mathrm{fi}}; \boldsymbol{\theta}) \end{cases} . \tag{16}$$

Detailed derivations of Eq. (16) is provided in App. H.4. Unlike identity and sigmoid transformation monotonically decreasing  $\boldsymbol{w}$  based solely on the absolute magnitude of the loss, the softmax updates weights based on the relative value of the loss. This ensures that the model does not assign extremely low weights to all data points. Specifically, the softmax transformation uses the weighted average loss as a reference: if the loss of a data point is below the reference, its weight increases; otherwise, its weight decreases. Moreover, since  $\mathcal{D}_{\rm ft}^{\rm benign}$  aligns more closely with  $\mathcal{D}_{\rm safe}$  than  $\mathcal{D}_{\rm ft}^{\rm harmful}$ , the benign data exhibits relatively lower loss, leading to an increase in their weights (see Fig. 5).

**Time-weighted accumulation of posterior bias.** We further explore weight suboptimality under identity transformation through the theoretical perspective of posterior bias, a newly proposed concept with detailed formulation and analysis in Apps. I.1 to I.5. Here, we only present the core theorem below (Detailed proof is provided in App. I.6):

**Theorem 4.2** (Time-Weighted Accumulation of Posterior Bias). Let  $(Tr_{\boldsymbol{w}}, Tr_{\boldsymbol{\theta}})$  and  $(Tr_{\boldsymbol{w}^*}, Tr_{\boldsymbol{\theta}^*})$  denote the SGLD sampling trajectories under identity transformation drawn from the target distributions  $p(\boldsymbol{w}, \boldsymbol{\theta} \mid \mathcal{D}_{\mathrm{ft}}, \mathcal{D}_{\mathrm{safe}})$  and  $p(\boldsymbol{w}^*, \boldsymbol{\theta}^* \mid \mathcal{D}_{\mathrm{ft}}, \mathcal{D}_{\mathrm{safe}}, \mathcal{D}_{\mathrm{ft}}^{\mathrm{val}})$ , respectively. Here,  $\mathcal{D}_{\mathrm{ft}}^{\mathrm{val}}$  is a held-out clean tuning dataset, serving as a test or validation set to evaluate fine-tuning performance. Then, the following proportionality holds:

$$\underbrace{\mathbb{E}_{\mathbf{T}_{\boldsymbol{w}}, \mathbf{Tr}_{\boldsymbol{w}^*}} \left\| \boldsymbol{w}^{(T)} - \boldsymbol{w}^{*(T)} \right\|}_{\mathcal{PB}^{(T)}} \propto \underbrace{\mathbb{E}_{\mathbf{T}_{\boldsymbol{\overline{w}}}, \mathbf{Tr}_{\boldsymbol{\overline{w}}^*}} \sum_{t=0}^{T-1} (T-t) \left\| \boldsymbol{w}^{(t)} - \boldsymbol{w}^{*(t)} \right\|}_{\sum_{t=1}^{T-1} (T-t) \mathcal{PB}^{(t)}}.$$
(17)

Here,  $\mathcal{PB}^{(T)}$  quantifies the posterior bias at iteration T, and summation  $\sum_{t=1}^{T-1} (T-t)\mathcal{PB}^{(t)}$  characterizes the cumulative posterior bias over the entire sampling trajectory.

**Remark.** Notably, the time-weighted factor T-t highlights the greater influence of earlier iterations on the cumulative bias, suggesting that suboptimal sampling in the early stages of the SGLD trajectory can propagate and aggressively impact the overall posterior inference.

# 5 Experiment

**Datasets and models.** Our experimental setup primarily follows [29, 33] to ensure fair comparison. For the alignment dataset ( $\mathcal{D}_{\text{safe}}$ , consisting of harmful prompt-safe answer pairs), we use the dataset

Table 1: Comparison with SOTA baselines, ( $|\mathcal{D}_{safe}| = 1000$  and  $|\mathcal{D}_{ft}| = 1000$  for BDS).

				Harmful Score ↓						Finetune Accuracy ↑					
Method	$\mathcal{D}_{\mathrm{safe}}$	$\mathcal{D}_{\mathrm{harmful}}$	clean	p=0.05	p=0.1	p=0.15	p=0.2	Average	clean	p=0.05	p=0.1	p=0.15	p=0.2	Average	
SFT	1	Х	1.30	21.90	33.70	49.30	61.70	33.58	81.54	91.74	93.12	92.66	92.89	90.39	
Lisa	/	×	0.90	14.50	23.7	31.20	39.10	21.88	86.93	91.86	92.32	92.20	92.32	91.13	
Repnoise	/	/	1.20	20.70	32.10	45.60	55.50	31.02	90.25	92.89	93.00	92.89	92.89	92.38	
Vaccine	/	/	1.30	12.10	28.3	44.10	55.20	28.20	90.83	93.58	93.69	93.23	93.23	92.91	
Booster	/	/	1.90	4.80	8.30	14.20	25.50	10.94	92.89	92.32	93.23	93.35	93.35	93.03	
BDS	✓	Х	1.10	1.60	1.20	1.50	1.30	1.34	93.81	94.04	93.69	93.92	93.69	93.83	

Table 2: Robustness for large harmful ratios p.

Method		Harmful Score ↓							Finetune Accuracy ↑							
	p=0.3	p=0.4	p=0.5	p=0.6	p=0.7	p=0.8	p=0.9	p=1.0	p=0.3	p=0.4	p=0.5	p=0.6	p=0.7	p=0.8	p=0.9	p=1.0
Booster	40.60	68.40	77.20	76.90	77.50	76.30	75.90	76.60	92.12	93.00	92.69	92.20	91.63	91.63	91.51	_
BDS	1.20	1.50	1.20	1.50	1.50	1.60	1.50	1.80	93.32	93.19	93.00	92.66	92.29	92.78	92.89	_

from [53], an enriched version of BeaverTails [36]. To simulate harmful fine-tuning attack, the fine-tuning dataset ( $\mathcal{D}_{\mathrm{ft}}$ ) is constructed by mixing a proportion p of unsafe data ( $\mathcal{D}_{\mathrm{ft}}^{\mathrm{harmful}}$ ) from BeaverTails with 1-p benign fine-tuning data ( $\mathcal{D}_{\mathrm{ft}}^{\mathrm{benign}}$ ), resulting in a total size of  $|\mathcal{D}_{\mathrm{ft}}|$ . Fine-tuning tasks are considered on SST2 [56], AGNEWS [80], GSM8K [9], AlpacaEval [38], and GEM benchmark. Model architectures include Llama2-7B [60], Gemma2-9B [59] and Qwen2-7B [74]. Default settings are p=0.1 and  $|\mathcal{D}_{\mathrm{ft}}|=1000$  ( $|\mathcal{D}_{\mathrm{ft}}|=700$  for AlpacaEval).

**Metrics.** We adopt two evaluation metrics for assessing model performance, following [29, 33]:

- Finetune Accuracy (FA): The accuracy on the testing dataset of the corresponding fine-tuning task.
   Details on evaluation procedure are provided in App. B.2.
- Harmful Score (HS): Using the moderation model from [36], we classify model outputs as harmful or non-harmful. The harmful score is defined as the proportion of unsafe outputs.

For harmful score calculation, we sample 1000 instructions from the testing set of BeaverTails [36]. Finetune accuracy is evaluated using 872, 1000, 1000, 1000 and 104 samples from the fine-tuning datasets SST2, AGNEWS, GSM8K, GEM, and AlpacaEval, respectively.

**Baselines.** We compare our method with five representative defense baselines, including the SOTA Booster [29], Vaccine [33], Repnoise [52], Lisa [31], and SFT (Supervised Fine-Tuning) [29]. Descriptions and implementation details of each baseline are provided in App. B.1.

**Implementation details.** For fine-tuning, we adopt LoRA [22] for efficient fine-tuning, following [29, 33, 21]. Fine-tuning is performed using the FusedAdam [50] with a learning rate of  $1 \times 10^{-5}$  and a weight decay of 0.1, as recommended by [29]. The training involves 20 epochs with a batch size of 10. The neural scheduler is implemented using a lightweight 125M Fairseq-Dense model [2] with an added trainable linear head. The scheduler's learning rate is set to  $5 \times 10^{-3}$  for scalar scheduler and  $1 \times 10^{-6}$  for neural scheduler. Unless otherwise specified, we use the scalar scheduler as default. More implementation details are provided in Apps. B.3 and B.4.

# 5.1 Main Results

Comparison with SOTA defense baselines. Tab. 1 presents comparison of BDS with several SOTA baselines across harmful ratios ranging from 0 to 0.2. BDS consistently outperforms all baselines in both defensive and fine-tuning performance, achieving a significant 9.60% reduction in average Harmful Score and a 0.8% improvement in average Finetune Accuracy. Existing baselines struggle to consistently mitigate harmful data influence: Simulation-based baselines like Booster and Vaccine enhance robustness by attack simulation, whose effectiveness diminishes significantly as the harmful ratio increases; RepNoise attempts to unlearn harmful knowledge but it inevitably recovers under higher harmful ratios; Lisa mixes alignment data with fine-tuning data but fundamentally lacks a deweighting mechanism and thus requires alignment data to scale with the unknown harmful ratio.

Notably, when the harmful ratio is 0 (i.e., benign attack [48]), BDS achieves the highest and well-preserved fine-tuning performance, whereas SFT suffers significant drops. This can be explained by the helpfulness-harmlessness trade-off: SFT endows the model with strong harmlessness after alignment but reduces its plasticity [11] to sufficiently adapt and learn helpfulness during fine-tuning, thus leading to lower fine-tuning accuracy. As the harmful ratio increases (e.g.,  $p:0\to0.2$ ), fine-tuning accuracy of SFT even rises because the introduced harmful data act as counterexamples

Table 3: Robustness across fine-tuning datasets Table 4: Robustness across model architectures ( $|\mathcal{D}_{\text{safe}}| = 1000$ ,  $|\mathcal{D}_{\text{ft}}| = 1000$ , p = 0.1). ( $|\mathcal{D}_{\text{safe}}| = 1000$ ,  $|\mathcal{D}_{\text{ft}}| = 1000$ , p = 0.1).

Method	SS	T2	AGI	News	GSN	И8K	Alp	oaca	Method	Lla	ma2	Gen	ma2	Qw	en2	Av	/g.
	HS↓	FA ↑		HS↓	FA ↑	HS↓	FA↑	HS↓	FA ↑	HS↓	FA ↑						
SFT	33.70	93.12	30.70	85.90	14.80	15.20	40.70	45.67	SFT	33.70	93.12	64.30	94.50	25.50	94.84	41.17	94.15
Lisa	23.70	92.32	16.80	83.20	5.10	12.00	14.30	41.35	Lisa	23.70	92.32	30.80	94.04	9.50	93.92	21.33	93.43
Repnoise	32.10	93.00	27.30	85.50	16.60	16.10	36.50	41.83	Repnoise	32.10	93.00	63.60	94.50	33.90	94.61	43.20	94.04
Vaccine	28.30	93.69	25.20	86.10	3.70	15.30	43.40	44.71	Vaccine	28.30	93.69	45.00	93.69	16.80	92.55	30.03	93.31
Booster	8.30	93.23	7.10	87.20	6.40	17.10	36.70	45.19	Booster	8.30	93.23	11.20	93.69	1.60	95.64	7.03	94.19
BDS	1.20	93.69	1.10	89.10	2.00	18.30	2.30	48.08	BDS	1.20	93.69	1.30	94.50	0.90	94.72	1.13	94.30

Table 5: Robustness for different  $|\mathcal{D}_{\mathrm{ft}}|$ .

Method		Harmfu	ıl Score .	ļ	Finetune Accuracy ↑					
	500	1000	1500	2000	500	1000	1500	2000		
Booster	3.80	8.30	20.10	33.60	92.66	93.23	94.04	94.15		
BDS	1.20	1.20	0.90	1.20	93.35	93.69	93.12	94.28		

140	ic o.	. Koot	istiics	55 101	unic	ıcıı	$\nu_{\rm sate}$	١٠
Method		Harmful	Score ↓		F	inetune A	Accuracy	<b>↑</b>
1	100	500	1000	1500	100	500	1000	1500

Table 6: Debuggage for different | D .

Table 7: Effectiveness and transferability of neural scheduler.  $A \to B$  denotes that the neural scheduler is trained on dataset A and directly applied to assign data weights on dataset B. [HS/FA] (new\_ID/00D) denote metrics under in-domain and out-of-domain transfer settings.

62.20 **1.70** 

34.60

Method	SST2		$SST2 \rightarrow SS$	T2 (unseen)	$ $ SST2 $\rightarrow$ AGNEWS			
	HS	FA	HS(new_ID)	FA(new_ID)	HS(new_OOD)	FA(new_OOD)		
Scalar Scheduler			_		_			
Neural Scheduler	1.70	93.69	2.50	93.23	2.80	89.20		

that prompt the model to "unlearn" part of its harmlessness, thereby restoring plasticity and improving its capacity to learn helpfulness. Our method achieves a better helpfulness—harmlessness trade-off by jointly optimizing the safety alignment and fine-tuning objectives, as shown in Eq. (7). This joint optimization resembles a multi-task learning paradigm, which more effectively balances the competing objectives of harmlessness and helpfulness than the sequential learning paradigm used in SFT. Further discussions on the helpfulness—harmlessness trade-off are provided in App. F.2.

**Robustness for high harmful ratios.** Prior evaluations [29, 33] are limited to low harmful ratios, as existing methods struggle under high harmful ratios. To highlight our robustness, we conduct experiments under high harmful ratios ranging from 0.3 to 1.0. As shown in Tab. 2, BDS significantly surpasses the SOTA Booster across all tested ratios in both harmful score and fine-tuning accuracy. At high harmful ratios from 0.5 to 1.0, BDS achieves a significant reduction in harmful score by over 70% and delivers a near 1% improvement in fine-tuning accuracy. These results highlight the exceptional robustness and reliability of BDS, even under highly adversarial conditions.

Robustness for diverse fine-tuning tasks. To assess generalization, we evaluate BDS on four fine-tuning datasets in Tab. 3. Results show that BDS consistently maintains exceptionally low harmful scores (around 1) across all tasks, while existing baselines exhibit severe instability and poor generalization. For instance, while Vaccine achieves a harmful score of 3.7 on GSM8K, it catastrophically underperforms on AlpacaEval with a harmful score of 43.30. These results highlight BDS's adaptability and robustness to complex tasks like GSM8K and AlpacaEval while ensuring harmlessness. More experiments on complex text generation tasks are provided in App. D.6.

**Robustness for different model architectures.** To further assess generalization, we evaluate BDS on two SOTA architectures, Gemma2-9B and Qwen2-7B. Tab. 4 demonstrates BDS consistently achieves low harmful scores, while existing baselines exhibit severe instability. While Booster attains a harmful score of 1.6 on Qwen2-7B, it collapses on Gemma2-9B, surging to 11.2. These highlight BDS's adaptability, ensuring consistent SOTA performance across diverse model architectures.

Robustness for different sizes of  $|\mathcal{D}_{\mathrm{ft}}|$ . To validate robustness to  $|\mathcal{D}_{\mathrm{ft}}|$  size, we evaluate its impact while keeping  $|\mathcal{D}_{\mathrm{safe}}|$  and the harmful ratio p fixed by default. As shown in Tab. 5, existing baseline suffers a sharp decline in defensive performance as  $|\mathcal{D}_{\mathrm{ft}}|$  increases. Booster's harmful score surges dramatically from 3.8 to 33.6, exposing its inability to handle larger datasets. In contrast, BDS demonstrates strong robustness, maintaining a consistently low harmful score of around 1 regardless of  $|\mathcal{D}_{\mathrm{ft}}|$  size. This highlights BDS's reliability in defending harmful fine-tuning, even as dataset sizes scale substantially. Robustness for larger dataset size is also demonstrated in App. D.5.

**Robustness for different sizes of**  $|\mathcal{D}_{safe}|$ . To validate robustness to  $|\mathcal{D}_{safe}|$  size, we evaluate its impact while keeping  $|\mathcal{D}_{ft}|$  and p fixed by default. As shown in Tab. 6, existing baselines collapses as  $|\mathcal{D}_{safe}|$  decreases, with defensive performance deteriorating sharply. In contrast, BDS exhibits remarkable

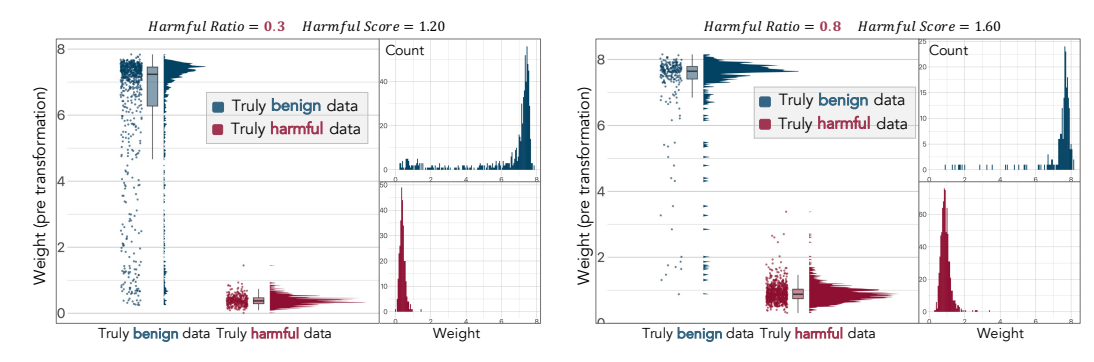


Figure 6: Data weights distributions across varying harmful ratios. More visualizations of weight distributions and scheduling dynamics are provided in Fig. 7 of App. D.1 and Fig. 8 of App. D.2.

resilience, consistently maintaining a harmful score below 2, even with only 100 alignment samples. These results underscore BDS's robustness in defense, even under limited alignment data.

Effectiveness and transferability of neural scheduler. To evaluate the effectiveness of the neural scheduler, we compare it with the scalar scheduler. The results in Tab. 7 show that the neural scheduler performs comparably to the scalar scheduler in both defensive and fine-tuning performance, achieving a harmful score below 2 on SST2. To further evaluate its transferability, we conduct experiments on unseen in-domain and out-of-domain datasets. The neural scheduler trained on the seen data is directly used to assign data weights to unseen data, which is subsequently employed for fine-tuning the LLM. As shown in Tab. 7, the neural scheduler generalizes effectively to both in-domain and out-of-domain unseen data, maintaining a harmful score below 3. These results highlight the strong effectiveness and transferability of the neural scheduler without the need for retraining, supporting its capacity to learn transferable data safety attributes [16].

Robustness for advanced attack: OOD and ISA. To evaluate the superior adaptiveness of our method under diverse attack dynamics, we conduct experiments against several challenging attack strategies: OOD attacks, and identity shifting attacks (ISA) [48]. Detailed results and discussions are provided in Apps. D.3 and D.4 due to limited space. Our approach significantly outperforms SOTA baselines, maintaining a low harmfulness ratio (around 1) across all attack strategies. This adaptiveness fundamentally stems from our loss-based data scheduling mechanism. Regardless of the attacker's strategy—whether OOD or ISA—harmful data tends to exhibit shared "unsafe behavior" (i.e., incurring higher loss within the loss landscape of safety-aware models [46]), thus being assigned with lower weights. This also mirrors the shared "safe behavior" observed across benign datasets (see Tab. 7), and supports the existence of transferable data safety attributes discussed in [16]. This mechanism enables our method to effectively adapt to various attack dynamics without explicit attack simulation.

**Visualization of adaptiveness.** Weight distributions (Fig. 6 and Fig. 7 in App. D.1) and scheduling dynamics (Fig. 8 in App. D.2) demonstrates BDS adaptively and correctly assigns higher weights to truly benign data and lower weights to truly harmful data, across varying harmful ratios.

Ablation studies on each component configuration are provided in detail in Apps. E.1 to E.3 and E.5.

**Discussion.** We offer comprehensive discussions on the adaptiveness of BDS, helpfulness-harmlessness trade-offs, limitations, and social impact in Apps. F.1 to F.5, F.7 and F.8, along with complexity and convergence analyses in Apps. G.1 and G.2.

### 6 Conclusion

We propose BDS, a novel and principled framework that achieves adaptive defense against harmful fine-tuning without requiring attack simulation. We introduce two implementations, Bayesian Scalar Scheduler and Amortized Bayesian Neural Scheduler, with the latter enabling efficient transfer to new data without retraining. Leveraging the post hoc nature of Bayesian inference, BDS learns the posterior distribution of data weights conditioned on the specific dataset, thus achieving adaptive defense. Extensive experiments confirm the SOTA performance and superior adaptiveness of BDS, significantly outperforming baselines by over 70% across diverse attack and defense settings.

# Acknowledgments

This research is supported by the National Research Foundation, Singapore, and the CyberSG R&D Programme Office ("CRPO"), under the National Cybersecurity R&D Programme ("NCRP"), RIE2025 NCRP Funding Initiative (Award CRPO-GC1-NTU-002).

## References

- [1] Alon Albalak, Yanai Elazar, Sang Michael Xie, Shayne Longpre, Nathan Lambert, Xinyi Wang, Niklas Muennighoff, Bairu Hou, Liangming Pan, Haewon Jeong, et al. A survey on data selection for language models. *arXiv preprint arXiv:2402.16827*, 2024.
- [2] Mikel Artetxe, Shruti Bhosale, Naman Goyal, Todor Mihaylov, Myle Ott, Sam Shleifer, Xi Victoria Lin, Jingfei Du, Srinivasan Iyer, Ramakanth Pasunuru, Giridharan Anantharaman, Xian Li, Shuohui Chen, Halil Akin, Mandeep Baines, Louis Martin, Xing Zhou, Punit Singh Koura, Brian O'Horo, Jeffrey Wang, Luke Zettlemoyer, Mona Diab, Zornitsa Kozareva, and Veselin Stoyanov. Efficient large scale language modeling with mixtures of experts. In Yoav Goldberg, Zornitsa Kozareva, and Yue Zhang, editors, *Proceedings of the 2022 Conference on Empirical Methods in Natural Language Processing*, pages 11699–11732, Abu Dhabi, United Arab Emirates, December 2022. Association for Computational Linguistics.
- [3] Federico Bianchi, Mirac Suzgun, Giuseppe Attanasio, Paul Röttger, Dan Jurafsky, Tatsunori Hashimoto, and James Zou. Safety-tuned llamas: Lessons from improving the safety of large language models that follow instructions. *arXiv preprint arXiv:2309.07875*, 2023.
- [4] Federico Bianchi, Mirac Suzgun, Giuseppe Attanasio, Paul Rottger, Dan Jurafsky, Tatsunori Hashimoto, and James Zou. Safety-tuned LLaMAs: Lessons from improving the safety of large language models that follow instructions. In *The Twelfth International Conference on Learning Representations*, 2024.
- [5] Hongyu Chen and Seraphina Goldfarb-Tarrant. Safer or luckier? Ilms as safety evaluators are not robust to artifacts. *arXiv preprint arXiv:2503.09347*, 2025.
- [6] Liang Chen, Xueting Han, Li Shen, Jing Bai, and Kam-Fai Wong. Beyond two-stage training: Cooperative sft and rl for llm reasoning. *arXiv preprint arXiv:2509.06948*, 2025.
- [7] Liang Chen, Xueting Han, Li Shen, Jing Bai, and Kam-Fai Wong. Vulnerability-aware alignment: Mitigating uneven forgetting in harmful fine-tuning, 2025.
- [8] Hyeong Kyu Choi, Xuefeng Du, and Yixuan Li. Safety-aware fine-tuning of large language models. *arXiv preprint arXiv:2410.10014*, 2024.
- [9] Karl Cobbe, Vineet Kosaraju, Mohammad Bavarian, Mark Chen, Heewoo Jun, Lukasz Kaiser, Matthias Plappert, Jerry Tworek, Jacob Hilton, Reiichiro Nakano, et al. Training verifiers to solve math word problems. *arXiv preprint arXiv:2110.14168*, 2021.
- [10] Zhijie Deng, Peng Cui, and Jun Zhu. Towards accelerated model training via bayesian data selection. Advances in Neural Information Processing Systems, 36:8513–8527, 2023.
- [11] Shibhansh Dohare, J. Fernando Hernandez-Garcia, Qingfeng Lan, Parash Rahman, A. Ruapm Mahmood, and Richard S. Sutton. Loss of plasticity in deep continual learning. *Nature*, 632:768—774, 2024.
- [12] Yanrui Du, Sendong Zhao, Danyang Zhao, Ming Ma, Yuhan Chen, Liangyu Huo, Qing Yang, Dongliang Xu, and Bing Qin. Mogu: A framework for enhancing safety of open-sourced llms while preserving their usability. *arXiv preprint arXiv:2405.14488*, 2024.
- [13] Heshan Fernando, Han Shen, Parikshit Ram, Yi Zhou, Horst Samulowitz, Nathalie Baracaldo, and Tianyi Chen. Mitigating forgetting in llm supervised fine-tuning and preference learning. arXiv preprint arXiv:2410.15483, 2024.

- [14] Samuel Gehman, Suchin Gururangan, Maarten Sap, Yejin Choi, and Noah A Smith. Real-toxicityprompts: Evaluating neural toxic degeneration in language models. *arXiv preprint* arXiv:2009.11462, 2020.
- [15] Jiawei Gu, Xuhui Jiang, Zhichao Shi, Hexiang Tan, Xuehao Zhai, Chengjin Xu, Wei Li, Yinghan Shen, Shengjie Ma, Honghao Liu, et al. A survey on llm-as-a-judge. *arXiv preprint arXiv:2411.15594*, 2024.
- [16] Yuxian Gu, Li Dong, Hongning Wang, Yaru Hao, Qingxiu Dong, Furu Wei, and Minlie Huang. Data selection via optimal control for language models. arXiv preprint arXiv:2410.07064, 2024.
- [17] Xingang Guo, Fangxu Yu, Huan Zhang, Lianhui Qin, and Bin Hu. Cold-attack: Jailbreaking Ilms with stealthiness and controllability. arXiv preprint arXiv:2402.08679, 2024.
- [18] Danny Halawi, Alexander Wei, Eric Wallace, Tony T Wang, Nika Haghtalab, and Jacob Steinhardt. Covert malicious finetuning: Challenges in safeguarding llm adaptation. *arXiv* preprint arXiv:2406.20053, 2024.
- [19] Moritz Hardt and Yu Sun. Test-time training on nearest neighbors for large language models. *arXiv preprint arXiv:2305.18466*, 2023.
- [20] Luxi He, Mengzhou Xia, and Peter Henderson. What's in your" safe" data?: Identifying benign data that breaks safety. *arXiv preprint arXiv:2404.01099*, 2024.
- [21] Chia-Yi Hsu, Yu-Lin Tsai, Chih-Hsun Lin, Pin-Yu Chen, Chia-Mu Yu, and Chun-Ying Huang. Safe lora: the silver lining of reducing safety risks when fine-tuning large language models, 2024.
- [22] Edward J Hu, Yelong Shen, Phillip Wallis, Zeyuan Allen-Zhu, Yuanzhi Li, Shean Wang, Lu Wang, and Weizhu Chen. Lora: Low-rank adaptation of large language models. *arXiv* preprint arXiv:2106.09685, 2021.
- [23] Zixuan Hu, Li Shen, Zhenyi Wang, Tongliang Liu, Chun Yuan, and Dacheng Tao. Architecture, dataset and model-scale agnostic data-free meta-learning. In *Proceedings of the IEEE/CVF Conference on Computer Vision and Pattern Recognition*, pages 7736–7745, 2023.
- [24] Zixuan Hu, Li Shen, Zhenyi Wang, Baoyuan Wu, Chun Yuan, and Dacheng Tao. Learning to learn from apis: Black-box data-free meta-learning. In *International Conference on Machine Learning*, pages 13610–13627. PMLR, 2023.
- [25] Zixuan Hu, Yongxian Wei, Li Shen, Zhenyi Wang, Lei Li, Chun Yuan, and Dacheng Tao. Sparse model inversion: Efficient inversion of vision transformers for data-free applications. In *Forty-first International Conference on Machine Learning*, 2024.
- [26] Zixuan Hu, Yongxian Wei, Li Shen, Zhenyi Wang, Baoyuan Wu, Chun Yuan, and Dacheng Tao. Task-distributionally robust data-free meta-learning. *IEEE Transactions on Pattern Analysis and Machine Intelligence*, 2025.
- [27] Zixuan Hu, Yongxian Wei, Li Shen, Chun Yuan, and Dacheng Tao. Lora recycle: Unlocking tuning-free few-shot adaptability in visual foundation models by recycling pre-tuned loras. In Proceedings of the Computer Vision and Pattern Recognition Conference, pages 25026–25037, 2025.
- [28] Tiansheng Huang, Gautam Bhattacharya, Pratik Joshi, Josh Kimball, and Ling Liu. Antidote: Post-fine-tuning safety alignment for large language models against harmful fine-tuning. *arXiv* preprint arXiv:2408.09600, 2024.
- [29] Tiansheng Huang, Sihao Hu, Fatih Ilhan, Selim Furkan Tekin, and Ling Liu. Booster: Tackling harmful fine-tuning for large language models via attenuating harmful perturbation. *arXiv* preprint arXiv:2409.01586, 2024.
- [30] Tiansheng Huang, Sihao Hu, Fatih Ilhan, Selim Furkan Tekin, and Ling Liu. Harmful fine-tuning attacks and defenses for large language models: A survey. arXiv preprint arXiv:2409.18169, 2024.

- [31] Tiansheng Huang, Sihao Hu, Fatih Ilhan, Selim Furkan Tekin, and Ling Liu. Lisa: Lazy safety alignment for large language models against harmful fine-tuning attack. In *The Thirty-eighth Annual Conference on Neural Information Processing Systems*, 2024.
- [32] Tiansheng Huang, Sihao Hu, Fatih Ilhan, Selim Furkan Tekin, and Ling Liu. Virus: Harmful fine-tuning attack for large language models bypassing guardrail moderation. *arXiv* preprint *arXiv*:2501.17433, 2025.
- [33] Tiansheng Huang, Sihao Hu, and Ling Liu. Vaccine: Perturbation-aware alignment for large language models against harmful fine-tuning attack. In *The Thirty-eighth Annual Conference on Neural Information Processing Systems*, 2024.
- [34] Jonas Hübotter, Sascha Bongni, Ido Hakimi, and Andreas Krause. Efficiently learning at test-time: Active fine-tuning of llms. *arXiv preprint arXiv:2410.08020*, 2024.
- [35] Jiaming Ji, Mickel Liu, Josef Dai, Xuehai Pan, Chi Zhang, Ce Bian, Boyuan Chen, Ruiyang Sun, Yizhou Wang, and Yaodong Yang. Beavertails: Towards improved safety alignment of Ilm via a human-preference dataset. *Advances in Neural Information Processing Systems*, 36, 2024.
- [36] Jiaming Ji, Mickel Liu, Juntao Dai, Xuehai Pan, Chi Zhang, Ce Bian, Ruiyang Sun, Yizhou Wang, and Yaodong Yang. Beavertails: Towards improved safety alignment of llm via a human-preference dataset. *arXiv preprint arXiv:2307.04657*, 2023.
- [37] Chak Tou Leong, Yi Cheng, Kaishuai Xu, Jian Wang, Hanlin Wang, and Wenjie Li. No two devils alike: Unveiling distinct mechanisms of fine-tuning attacks. arXiv preprint arXiv:2405.16229, 2024.
- [38] Xuechen Li, Tianyi Zhang, Yann Dubois, Rohan Taori, Ishaan Gulrajani, Carlos Guestrin, Percy Liang, and Tatsunori B. Hashimoto. Alpacaeval: An automatic evaluator of instruction-following models. https://github.com/tatsu-lab/alpaca\_eval, 2023.
- [39] Zhe Li, Wei Zhao, Yige Li, and Jun Sun. Do influence functions work on large language models? *arXiv preprint arXiv:2409.19998*, 2024.
- [40] Guozhi Liu, Weiwei Lin, Qi Mu, Tiansheng Huang, Ruichao Mo, Yuren Tao, and Li Shen. Targeted vaccine: Safety alignment for large language models against harmful fine-tuning via layer-wise perturbation. *IEEE Transactions on Information Forensics and Security*, 2025.
- [41] Guozhi Liu, Qi Mu, Tiansheng Huang, Xinhua Wang, Li Shen, Weiwei Lin, and Zhang Li. Pharmacist: Safety alignment data curation for large language models against harmful fine-tuning. *arXiv preprint arXiv:2510.10085*, 2025.
- [42] Xiaoqun Liu, Jiacheng Liang, Luoxi Tang, Muchao Ye, Weicheng Ma, and Zhaohan Xi. Data to defense: The role of curation in customizing llms against jailbreaking attacks. *arXiv preprint arXiv:2410.02220*, 2024.
- [43] Michael McCloskey and Neal J Cohen. Catastrophic interference in connectionist networks: The sequential learning problem. In *Psychology of learning and motivation*, volume 24, pages 109–165. Elsevier, 1989.
- [44] Jishnu Mukhoti, Yarin Gal, Philip HS Torr, and Puneet K Dokania. Fine-tuning can cripple your foundation model; preserving features may be the solution. *arXiv preprint arXiv:2308.13320*, 2023.
- [45] Christopher Nemeth and Paul Fearnhead. Stochastic gradient markov chain monte carlo. *Journal of the American Statistical Association*, 116(533):433–450, 2021.
- [46] Sheng Yun Peng, Pin-Yu Chen, Matthew Hull, and Duen Horng Chau. Navigating the safety land-scape: Measuring risks in finetuning large language models. *arXiv preprint arXiv:2405.17374*, 2024.
- [47] Sheng Yun Peng, Weilin Xu, Cory Cornelius, Matthew Hull, Kevin Li, Rahul Duggal, Mansi Phute, Jason Martin, and Duen Horng Chau. Robust principles: Architectural design principles for adversarially robust cnns. *arXiv preprint arXiv:2308.16258*, 2023.

- [48] Xiangyu Qi, Yi Zeng, Tinghao Xie, Pin-Yu Chen, Ruoxi Jia, Prateek Mittal, and Peter Henderson. Fine-tuning aligned language models compromises safety, even when users do not intend to! In *The Twelfth International Conference on Learning Representations*, 2024.
- [49] Lianhui Qin, Sean Welleck, Daniel Khashabi, and Yejin Choi. Cold decoding: Energy-based constrained text generation with langevin dynamics. Advances in Neural Information Processing Systems, 35:9538–9551, 2022.
- [50] Jeff Rasley, Samyam Rajbhandari, Olatunji Ruwase, and Yuxiong He. Deepspeed: System optimizations enable training deep learning models with over 100 billion parameters. In *Proceedings of the 26th ACM SIGKDD International Conference on Knowledge Discovery & Data Mining*, pages 3505–3506, 2020.
- [51] Sachin Ravi and Alex Beatson. Amortized bayesian meta-learning. In *International Conference on Learning Representations*, 2019.
- [52] Domenic Rosati, Jan Wehner, Kai Williams, Łukasz Bartoszcze, David Atanasov, Robie Gonzales, Subhabrata Majumdar, Carsten Maple, Hassan Sajjad, and Frank Rudzicz. Representation noising effectively prevents harmful fine-tuning on llms. arXiv preprint arXiv:2405.14577, 2024.
- [53] Domenic Rosati, Jan Wehner, Kai Williams, Łukasz Bartoszcze, Jan Batzner, Hassan Saj-jad, and Frank Rudzicz. Immunization against harmful fine-tuning attacks. *arXiv* preprint arXiv:2402.16382, 2024.
- [54] Paul Röttger, Hannah Rose Kirk, Bertie Vidgen, Giuseppe Attanasio, Federico Bianchi, and Dirk Hovy. Xstest: A test suite for identifying exaggerated safety behaviours in large language models. arXiv preprint arXiv:2308.01263, 2023.
- [55] Han Shen, Pin-Yu Chen, Payel Das, and Tianyi Chen. Seal: Safety-enhanced aligned llm fine-tuning via bilevel data selection. *arXiv preprint arXiv:2410.07471*, 2024.
- [56] Richard Socher, Alex Perelygin, Jean Wu, Jason Chuang, Christopher D Manning, Andrew Y Ng, and Christopher Potts. Recursive deep models for semantic compositionality over a sentiment treebank. In *Proceedings of the 2013 conference on empirical methods in natural language processing*, pages 1631–1642, 2013.
- [57] Rishub Tamirisa, Bhrugu Bharathi, Long Phan, Andy Zhou, Alice Gatti, Tarun Suresh, Maxwell Lin, Justin Wang, Rowan Wang, Ron Arel, et al. Tamper-resistant safeguards for open-weight llms. *arXiv* preprint arXiv:2408.00761, 2024.
- [58] Rishub Tamirisa, Bhrugu Bharathi, Long Phan, Andy Zhou, Alice Gatti, Tarun Suresh, Maxwell Lin, Justin Wang, Rowan Wang, Ron Arel, Andy Zou, Dawn Song, Bo Li, Dan Hendrycks, and Mantas Mazeika. Tamper-resistant safeguards for open-weight LLMs. In *The Thirteenth International Conference on Learning Representations*, 2025.
- [59] Gemma Team, Thomas Mesnard, Cassidy Hardin, Robert Dadashi, Surya Bhupatiraju, Shreya Pathak, Laurent Sifre, Morgane Rivière, Mihir Sanjay Kale, Juliette Love, et al. Gemma: Open models based on gemini research and technology. arXiv preprint arXiv:2403.08295, 2024.
- [60] Hugo Touvron, Thibaut Lavril, Gautier Izacard, Xavier Martinet, Marie-Anne Lachaux, Timothée Lacroix, Baptiste Rozière, Naman Goyal, Eric Hambro, Faisal Azhar, et al. Llama: Open and efficient foundation language models. *arXiv preprint arXiv:2302.13971*, 2023.
- [61] Jiongxiao Wang, Jiazhao Li, Yiquan Li, Xiangyu Qi, Junjie Hu, Yixuan Li, Patrick McDaniel, Muhao Chen, Bo Li, and Chaowei Xiao. Mitigating fine-tuning based jailbreak attack with backdoor enhanced safety alignment. *arXiv preprint arXiv:2402.14968*, 2024.
- [62] Yibo Wang, Tiansheng Huang, Li Shen, Huanjin Yao, Haotian Luo, Rui Liu, Naiqiang Tan, Jiaxing Huang, and Dacheng Tao. Panacea: Mitigating harmful fine-tuning for large language models via post-fine-tuning perturbation. *Advances in Neural Information Processing Systems*, 2025.

- [63] Zhichao Wang, Bin Bi, Zixu Zhu, Xiangbo Mao, Jun Wang, and Shiyu Wang. Uft: Unifying fine-tuning of sft and rlhf/dpo/una through a generalized implicit reward function. arXiv preprint arXiv:2410.21438, 2024.
- [64] Yongxian Wei, Runxi Cheng, Weike Jin, Enneng Yang, Li Shen, Lu Hou, Sinan Du, Chun Yuan, Xiaochun Cao, and Dacheng Tao. Unifying multimodal large language model capabilities and modalities via model merging. *arXiv preprint arXiv:2505.19892*, 2025.
- [65] Yongxian Wei, Zixuan Hu, Li Shen, Zhenyi Wang, Yu Li, Chun Yuan, and Dacheng Tao. Task groupings regularization: Data-free meta-learning with heterogeneous pre-trained models. In Ruslan Salakhutdinov, Zico Kolter, Katherine Heller, Adrian Weller, Nuria Oliver, Jonathan Scarlett, and Felix Berkenkamp, editors, *Proceedings of the 41st International Conference on Machine Learning*, volume 235 of *Proceedings of Machine Learning Research*, pages 52573–52587. PMLR, 21–27 Jul 2024.
- [66] Yongxian Wei, Zixuan Hu, Li Shen, Zhenyi Wang, Chun Yuan, and Dacheng Tao. Open-vocabulary customization from clip via data-free knowledge distillation. In *The Thirteenth International Conference on Learning Representations*, 2025.
- [67] Yongxian Wei, Zixuan Hu, Zhenyi Wang, Li Shen, Chun Yuan, and Dacheng Tao. Free: Faster and better data-free meta-learning. In *Proceedings of the IEEE/CVF conference on computer vision and pattern recognition*, pages 23273–23282, 2024.
- [68] Yongxian Wei, Anke Tang, Li Shen, Zixuan Hu, Chun Yuan, and Xiaochun Cao. Modeling multi-task model merging as adaptive projective gradient descent. In *Forty-second International Conference on Machine Learning*, 2025.
- [69] Max Welling and Yee W Teh. Bayesian learning via stochastic gradient langevin dynamics. In *Proceedings of the 28th international conference on machine learning (ICML-11)*, pages 681–688. Citeseer, 2011.
- [70] Di Wu, Xin Lu, Yanyan Zhao, and Bing Qin. Separate the wheat from the chaff: A post-hoc approach to safety re-alignment for fine-tuned language models. arXiv preprint arXiv:2412.11041, 2024.
- [71] Mengzhou Xia, Sadhika Malladi, Suchin Gururangan, Sanjeev Arora, and Danqi Chen. Less: Selecting influential data for targeted instruction tuning. *arXiv preprint arXiv:2402.04333*, 2024.
- [72] Sang Michael Xie, Shibani Santurkar, Tengyu Ma, and Percy S Liang. Data selection for language models via importance resampling. Advances in Neural Information Processing Systems, 36:34201–34227, 2023.
- [73] Xinnuo Xu, Minyoung Kim, Royson Lee, Brais Martinez, and Timothy Hospedales. A bayesian approach to data point selection. Advances in Neural Information Processing Systems, 37:38171– 38198, 2024.
- [74] An Yang, Baosong Yang, Binyuan Hui, Bo Zheng, Bowen Yu, Chang Zhou, Chengpeng Li, Chengyuan Li, Dayiheng Liu, Fei Huang, et al. Qwen2 technical report. *arXiv* preprint *arXiv*:2407.10671, 2024.
- [75] Biao Yi, Tiansheng Huang, Baolei Zhang, Tong Li, Lihai Nie, Zheli Liu, and Li Shen. Ctrap: Embedding collapse trap to safeguard large language models from harmful fine-tuning. *arXiv* preprint arXiv:2505.16559, 2025.
- [76] Xin Yi, Shunfan Zheng, Linlin Wang, Xiaoling Wang, and Liang He. A safety realignment framework via subspace-oriented model fusion for large language models. *Knowledge-Based Systems*, 306:112701, 2024.
- [77] Zichun Yu, Spandan Das, and Chenyan Xiong. Mates: Model-aware data selection for efficient pretraining with data influence models. *arXiv* preprint arXiv:2406.06046, 2024.

- [78] Shaokun Zhang, Xiaobo Xia, Zhaoqing Wang, Ling-Hao Chen, Jiale Liu, Qingyun Wu, and Tongliang Liu. Ideal: Influence-driven selective annotations empower in-context learners in large language models. *arXiv* preprint arXiv:2310.10873, 2023.
- [79] Wenxuan Zhang, Philip HS Torr, Mohamed Elhoseiny, and Adel Bibi. Bi-factorial preference optimization: Balancing safety-helpfulness in language models. arXiv preprint arXiv:2408.15313, 2024.
- [80] Xiang Zhang, Junbo Zhao, and Yann LeCun. Character-level convolutional networks for text classification. *Advances in neural information processing systems*, 28, 2015.
- [81] Xiaoyu Zhang, Juan Zhai, Shiqing Ma, Chao Shen, Tianlin Li, Weipeng Jiang, and Yang Liu. Speculative coreset selection for task-specific fine-tuning. arXiv preprint arXiv:2410.01296, 2024.
- [82] Zhi-Hua Zhou. Machine learning. Springer nature, 2021.
- [83] Yongshuo Zong, Ondrej Bohdal, Tingyang Yu, Yongxin Yang, and Timothy Hospedales. Safety fine-tuning at (almost) no cost: A baseline for vision large language models. *arXiv preprint arXiv:2402.02207*, 2024.
- [84] Andy Zou, Zifan Wang, J. Zico Kolter, and Matt Fredrikson. Universal and transferable adversarial attacks on aligned language models, 2023.
- [85] Difan Zou, Pan Xu, and Quanquan Gu. Faster convergence of stochastic gradient langevin dynamics for non-log-concave sampling. In *Uncertainty in Artificial Intelligence*, pages 1152–1162. PMLR, 2021.

# **NeurIPS Paper Checklist**

#### 1. Claims

Question: Do the main claims made in the abstract and introduction accurately reflect the paper's contributions and scope?

Answer: [Yes]

Justification: The claim is explicitly stated in the abstract and introduction, and is well supported by extensive experiments across diverse attack and defense scenarios.

#### Guidelines:

- The answer NA means that the abstract and introduction do not include the claims made in the paper.
- The abstract and/or introduction should clearly state the claims made, including the contributions made in the paper and important assumptions and limitations. A No or NA answer to this question will not be perceived well by the reviewers.
- The claims made should match theoretical and experimental results, and reflect how much the results can be expected to generalize to other settings.
- It is fine to include aspirational goals as motivation as long as it is clear that these goals are not attained by the paper.

#### 2. Limitations

Question: Does the paper discuss the limitations of the work performed by the authors?

Answer: [Yes]

Justification: See App. F.7.

#### Guidelines:

- The answer NA means that the paper has no limitation while the answer No means that the paper has limitations, but those are not discussed in the paper.
- The authors are encouraged to create a separate "Limitations" section in their paper.
- The paper should point out any strong assumptions and how robust the results are to violations of these assumptions (e.g., independence assumptions, noiseless settings, model well-specification, asymptotic approximations only holding locally). The authors should reflect on how these assumptions might be violated in practice and what the implications would be.
- The authors should reflect on the scope of the claims made, e.g., if the approach was only tested on a few datasets or with a few runs. In general, empirical results often depend on implicit assumptions, which should be articulated.
- The authors should reflect on the factors that influence the performance of the approach. For example, a facial recognition algorithm may perform poorly when image resolution is low or images are taken in low lighting. Or a speech-to-text system might not be used reliably to provide closed captions for online lectures because it fails to handle technical jargon.
- The authors should discuss the computational efficiency of the proposed algorithms and how they scale with dataset size.
- If applicable, the authors should discuss possible limitations of their approach to address problems of privacy and fairness.
- While the authors might fear that complete honesty about limitations might be used by reviewers as grounds for rejection, a worse outcome might be that reviewers discover limitations that aren't acknowledged in the paper. The authors should use their best judgment and recognize that individual actions in favor of transparency play an important role in developing norms that preserve the integrity of the community. Reviewers will be specifically instructed to not penalize honesty concerning limitations.

# 3. Theory assumptions and proofs

Question: For each theoretical result, does the paper provide the full set of assumptions and a complete (and correct) proof?

Answer: [Yes]

Justification: Detailed derivations and proofs are provided in Apps. H.1 to H.4 and App. I.6. Guidelines:

- The answer NA means that the paper does not include theoretical results.
- All the theorems, formulas, and proofs in the paper should be numbered and cross-referenced.
- All assumptions should be clearly stated or referenced in the statement of any theorems.
- The proofs can either appear in the main paper or the supplemental material, but if they appear in the supplemental material, the authors are encouraged to provide a short proof sketch to provide intuition.
- Inversely, any informal proof provided in the core of the paper should be complemented by formal proofs provided in appendix or supplemental material.
- Theorems and Lemmas that the proof relies upon should be properly referenced.

## 4. Experimental result reproducibility

Question: Does the paper fully disclose all the information needed to reproduce the main experimental results of the paper to the extent that it affects the main claims and/or conclusions of the paper (regardless of whether the code and data are provided or not)?

Answer: [Yes]

Justification: Detailed implementation details are provided in App. B.1, App. B.3, App. B.2, and App. B.4.

#### Guidelines:

- The answer NA means that the paper does not include experiments.
- If the paper includes experiments, a No answer to this question will not be perceived well by the reviewers: Making the paper reproducible is important, regardless of whether the code and data are provided or not.
- If the contribution is a dataset and/or model, the authors should describe the steps taken to make their results reproducible or verifiable.
- Depending on the contribution, reproducibility can be accomplished in various ways. For example, if the contribution is a novel architecture, describing the architecture fully might suffice, or if the contribution is a specific model and empirical evaluation, it may be necessary to either make it possible for others to replicate the model with the same dataset, or provide access to the model. In general, releasing code and data is often one good way to accomplish this, but reproducibility can also be provided via detailed instructions for how to replicate the results, access to a hosted model (e.g., in the case of a large language model), releasing of a model checkpoint, or other means that are appropriate to the research performed.
- While NeurIPS does not require releasing code, the conference does require all submissions to provide some reasonable avenue for reproducibility, which may depend on the nature of the contribution. For example
- (a) If the contribution is primarily a new algorithm, the paper should make it clear how to reproduce that algorithm.
- (b) If the contribution is primarily a new model architecture, the paper should describe the architecture clearly and fully.
- (c) If the contribution is a new model (e.g., a large language model), then there should either be a way to access this model for reproducing the results or a way to reproduce the model (e.g., with an open-source dataset or instructions for how to construct the dataset).
- (d) We recognize that reproducibility may be tricky in some cases, in which case authors are welcome to describe the particular way they provide for reproducibility. In the case of closed-source models, it may be that access to the model is limited in some way (e.g., to registered users), but it should be possible for other researchers to have some path to reproducing or verifying the results.

#### 5. Open access to data and code

Question: Does the paper provide open access to the data and code, with sufficient instructions to faithfully reproduce the main experimental results, as described in supplemental material?

Answer: [Yes]

Justification: Code and instructions for reproducing all experiments will be released upon acceptance.

### Guidelines:

- The answer NA means that paper does not include experiments requiring code.
- Please see the NeurIPS code and data submission guidelines (https://nips.cc/public/guides/CodeSubmissionPolicy) for more details.
- While we encourage the release of code and data, we understand that this might not be possible, so "No" is an acceptable answer. Papers cannot be rejected simply for not including code, unless this is central to the contribution (e.g., for a new open-source benchmark).
- The instructions should contain the exact command and environment needed to run to reproduce the results. See the NeurIPS code and data submission guidelines (https://nips.cc/public/guides/CodeSubmissionPolicy) for more details.
- The authors should provide instructions on data access and preparation, including how
  to access the raw data, preprocessed data, intermediate data, and generated data, etc.
- The authors should provide scripts to reproduce all experimental results for the new proposed method and baselines. If only a subset of experiments are reproducible, they should state which ones are omitted from the script and why.
- At submission time, to preserve anonymity, the authors should release anonymized versions (if applicable).
- Providing as much information as possible in supplemental material (appended to the paper) is recommended, but including URLs to data and code is permitted.

### 6. Experimental setting/details

Question: Does the paper specify all the training and test details (e.g., data splits, hyper-parameters, how they were chosen, type of optimizer, etc.) necessary to understand the results?

Answer: [Yes]

Justification: Detailed implementation details are provided in App. B.1, App. B.3, App. B.2, and App. B.4.

## Guidelines:

- The answer NA means that the paper does not include experiments.
- The experimental setting should be presented in the core of the paper to a level of detail that is necessary to appreciate the results and make sense of them.
- The full details can be provided either with the code, in appendix, or as supplemental material.

## 7. Experiment statistical significance

Question: Does the paper report error bars suitably and correctly defined or other appropriate information about the statistical significance of the experiments?

Answer: [No]

Justification: In the community of LLM harmful fine-tuning defense [29, 33], it is common not to report error bars due to the high computational cost and the stability of results across runs.

- The answer NA means that the paper does not include experiments.
- The authors should answer "Yes" if the results are accompanied by error bars, confidence intervals, or statistical significance tests, at least for the experiments that support the main claims of the paper.
- The factors of variability that the error bars are capturing should be clearly stated (for example, train/test split, initialization, random drawing of some parameter, or overall run with given experimental conditions).

- The method for calculating the error bars should be explained (closed form formula, call to a library function, bootstrap, etc.)
- The assumptions made should be given (e.g., Normally distributed errors).
- It should be clear whether the error bar is the standard deviation or the standard error
  of the mean.
- It is OK to report 1-sigma error bars, but one should state it. The authors should preferably report a 2-sigma error bar than state that they have a 96% CI, if the hypothesis of Normality of errors is not verified.
- For asymmetric distributions, the authors should be careful not to show in tables or figures symmetric error bars that would yield results that are out of range (e.g. negative error rates).
- If error bars are reported in tables or plots, The authors should explain in the text how they were calculated and reference the corresponding figures or tables in the text.

## 8. Experiments compute resources

Question: For each experiment, does the paper provide sufficient information on the computer resources (type of compute workers, memory, time of execution) needed to reproduce the experiments?

Answer: [Yes]

Justification: All experiments were conducted on a single NVIDIA A100 40GB GPU. Details on computational requirements and complexity analysis are provided in App. G.1.

#### Guidelines:

- The answer NA means that the paper does not include experiments.
- The paper should indicate the type of compute workers CPU or GPU, internal cluster, or cloud provider, including relevant memory and storage.
- The paper should provide the amount of compute required for each of the individual experimental runs as well as estimate the total compute.
- The paper should disclose whether the full research project required more compute than the experiments reported in the paper (e.g., preliminary or failed experiments that didn't make it into the paper).

#### 9. Code of ethics

Question: Does the research conducted in the paper conform, in every respect, with the NeurIPS Code of Ethics https://neurips.cc/public/EthicsGuidelines?

Answer: [Yes]

Justification: Our research fully complies with the NeurIPS Code of Ethics.

#### Guidelines:

- The answer NA means that the authors have not reviewed the NeurIPS Code of Ethics.
- If the authors answer No, they should explain the special circumstances that require a
  deviation from the Code of Ethics.
- The authors should make sure to preserve anonymity (e.g., if there is a special consideration due to laws or regulations in their jurisdiction).

## 10. Broader impacts

Question: Does the paper discuss both potential positive societal impacts and negative societal impacts of the work performed?

Answer: [Yes]

Justification: See App. F.8.

- The answer NA means that there is no societal impact of the work performed.
- If the authors answer NA or No, they should explain why their work has no societal impact or why the paper does not address societal impact.

- Examples of negative societal impacts include potential malicious or unintended uses (e.g., disinformation, generating fake profiles, surveillance), fairness considerations (e.g., deployment of technologies that could make decisions that unfairly impact specific groups), privacy considerations, and security considerations.
- The conference expects that many papers will be foundational research and not tied to particular applications, let alone deployments. However, if there is a direct path to any negative applications, the authors should point it out. For example, it is legitimate to point out that an improvement in the quality of generative models could be used to generate deepfakes for disinformation. On the other hand, it is not needed to point out that a generic algorithm for optimizing neural networks could enable people to train models that generate Deepfakes faster.
- The authors should consider possible harms that could arise when the technology is being used as intended and functioning correctly, harms that could arise when the technology is being used as intended but gives incorrect results, and harms following from (intentional or unintentional) misuse of the technology.
- If there are negative societal impacts, the authors could also discuss possible mitigation strategies (e.g., gated release of models, providing defenses in addition to attacks, mechanisms for monitoring misuse, mechanisms to monitor how a system learns from feedback over time, improving the efficiency and accessibility of ML).

## 11. Safeguards

Question: Does the paper describe safeguards that have been put in place for responsible release of data or models that have a high risk for misuse (e.g., pretrained language models, image generators, or scraped datasets)?

Answer: [NA]

Justification: The paper poses no such risks.

#### Guidelines:

- The answer NA means that the paper poses no such risks.
- Released models that have a high risk for misuse or dual-use should be released with necessary safeguards to allow for controlled use of the model, for example by requiring that users adhere to usage guidelines or restrictions to access the model or implementing safety filters.
- Datasets that have been scraped from the Internet could pose safety risks. The authors should describe how they avoided releasing unsafe images.
- We recognize that providing effective safeguards is challenging, and many papers do
  not require this, but we encourage authors to take this into account and make a best
  faith effort.

### 12. Licenses for existing assets

Question: Are the creators or original owners of assets (e.g., code, data, models), used in the paper, properly credited and are the license and terms of use explicitly mentioned and properly respected?

Answer: [Yes]

Justification: We use publicly available datasets and models with proper citation, and adhere to their respective licenses.

- The answer NA means that the paper does not use existing assets.
- The authors should cite the original paper that produced the code package or dataset.
- The authors should state which version of the asset is used and, if possible, include a URL.
- The name of the license (e.g., CC-BY 4.0) should be included for each asset.
- For scraped data from a particular source (e.g., website), the copyright and terms of service of that source should be provided.

- If assets are released, the license, copyright information, and terms of use in the
  package should be provided. For popular datasets, paperswithcode.com/datasets
  has curated licenses for some datasets. Their licensing guide can help determine the
  license of a dataset.
- For existing datasets that are re-packaged, both the original license and the license of the derived asset (if it has changed) should be provided.
- If this information is not available online, the authors are encouraged to reach out to the asset's creators.

#### 13. New assets

Question: Are new assets introduced in the paper well documented and is the documentation provided alongside the assets?

Answer: [NA]

Justification: The paper does not release new assets.

#### Guidelines:

- The answer NA means that the paper does not release new assets.
- Researchers should communicate the details of the dataset/code/model as part of their submissions via structured templates. This includes details about training, license, limitations, etc.
- The paper should discuss whether and how consent was obtained from people whose asset is used.
- At submission time, remember to anonymize your assets (if applicable). You can either create an anonymized URL or include an anonymized zip file.

## 14. Crowdsourcing and research with human subjects

Question: For crowdsourcing experiments and research with human subjects, does the paper include the full text of instructions given to participants and screenshots, if applicable, as well as details about compensation (if any)?

Answer: [NA]

Justification: The paper does not involve crowdsourcing nor research with human subjects.

# Guidelines:

- The answer NA means that the paper does not involve crowdsourcing nor research with human subjects.
- Including this information in the supplemental material is fine, but if the main contribution of the paper involves human subjects, then as much detail as possible should be included in the main paper.
- According to the NeurIPS Code of Ethics, workers involved in data collection, curation, or other labor should be paid at least the minimum wage in the country of the data collector.

# 15. Institutional review board (IRB) approvals or equivalent for research with human subjects

Question: Does the paper describe potential risks incurred by study participants, whether such risks were disclosed to the subjects, and whether Institutional Review Board (IRB) approvals (or an equivalent approval/review based on the requirements of your country or institution) were obtained?

Answer: [NA]

Justification: The paper does not involve crowdsourcing nor research with human subjects. Guidelines:

- The answer NA means that the paper does not involve crowdsourcing nor research with human subjects.
- Depending on the country in which research is conducted, IRB approval (or equivalent) may be required for any human subjects research. If you obtained IRB approval, you should clearly state this in the paper.

- We recognize that the procedures for this may vary significantly between institutions and locations, and we expect authors to adhere to the NeurIPS Code of Ethics and the guidelines for their institution.
- For initial submissions, do not include any information that would break anonymity (if applicable), such as the institution conducting the review.

## 16. Declaration of LLM usage

Question: Does the paper describe the usage of LLMs if it is an important, original, or non-standard component of the core methods in this research? Note that if the LLM is used only for writing, editing, or formatting purposes and does not impact the core methodology, scientific rigorousness, or originality of the research, declaration is not required.

Answer: [NA]

Justification: The core method development in this research does not involve LLMs as any important, original, or non-standard components.

- The answer NA means that the core method development in this research does not involve LLMs as any important, original, or non-standard components.
- Please refer to our LLM policy (https://neurips.cc/Conferences/2025/LLM) for what should or should not be described.

# Appendix of Adaptive Defense against Harmful Fine-Tuning for Large Language Models via Bayesian Data Scheduler

# **Contents**

A	Rela	ated Work	25
В	Mor	re Details	26
	B.1	Details on Baselines	26
	B.2	Details on Fine-Tuning Task Evaluation	27
	B.3	Details on Scheduler Training	27
	B.4	Details on Fine-Tuning	27
C	Algo	prithms	28
D	Mor	re Experiments	28
	D.1	Weight Distribution of Benign and Harmful Data under Various Harmful Ratios	28
	D.2	Scheduling Dynamics for Benign and Harmful Data under Various Harmful Ratios	28
	D.3	Robustness for OOD Attack	31
	D.4	Robustness for Identify Shifting Attack (ISA) [48]	31
	D.5	Robustness for Larger Fine-Tuning Dataset Size	31
	D.6	Robustness on More Complex Tasks: Data-to-Text Generation	32
	D.7	Comparison with Detection-Based Methods	32
	D.8	Comparison with Deterministic Data Curation Methods	32
E	Abla	ation Studies	33
	E.1	Impact of Different Weight Transformations	33
	E.2	Impact of Different Weight Priors	33
	E.3	Impact of Weight Initialization	33
	E.4	Impact of the Alignment Dataset	34
	E.5	Impact of the Data Weight	34
F	Mor	re Discussions	34
	F.1	Insights into Adaptiveness to Diverse Attack Dynamics	34
	F.2	Insights into Helpfulness-Harmlessness Trade-Offs	35
	F.3	Simulation-Free vs. Simulation-Based Defense	35
	F.4	Data Scheduling vs. Data Filtering	35
	F.5	Over-Refusal	36
	F.6	Zero-Shot Performance	36
	E 7	Limitation and Future Work	36

	F.8	Impact Statement	37
G	Mor	e Analyses	37
	G.1	Time and Space Complexity Analysis	37
	G.2	Convergence Analysis of SGLD Sampling	38
Н	Deri	vation of Equations	39
	H.1	Derivation of Eq. (1)	39
	H.2	Derivation of Eq. (4)	39
	H.3	Derivation of Eq. (10)	١(
	H.4	Derivation of Eq. (16)	1(
Ι	Con	cept of Posterior Bias	<b>1</b> 1
	I.1	Motivation of Proposed Posterior Bias	<b>ļ</b> 1
	I.2	Definition of Posterior Bias	<b>ļ</b> ]
	I.3	Empirical Posterior Bias with SGLD Sampling	<b>ļ</b> ]
	I.4	Understanding Posterior Bias under Identity Weight Transformation	12
	I.5	Theorem of Time-Weighted Accumulation of Posterior Bias	12
	I.6	Proof of theorem Theorem 4.2	13

### A Related Work

Fine-tuning-as-a-service has become a widely adopted paradigm among mainstream LLM providers (e.g., OpenAI<sup>4</sup> and Mistral<sup>5</sup>). Recent red teaming studies [48, 29, 30] have revealed a critical vulnerability: harmful fine-tuning. Harmful fine-tuning refers to that the presence of even a small fraction of harmful data in user- provided datasets can cause fine-tuned models to deviate from the safety alignment established during pre-training, i.e., the model forgets to give refusal answer towards harmful prompts after fine-tuning on a few harmful samples.

Mechanism study of harmful fine-tuning. Existing research has made efforts to analyze the mechanisms underlying the high sensitivity of LLMs to harmful fine-tuning. (i) Adversarial permutations: One line of work reveals that harmful fine-tuning can induce adversarial perturbations to the model, to which LLMs are highly sensitive. For instance, Vicanne [33] demonstrates that tuning with harmful data in user-provided datasets can cause embedding drift. Similarly, Booster [29] identifies that harmful fine-tuning leads to parameter perturbations. Moreover, [46] introduces the concept of a safety basin, wherein LLMs can tolerate parameter perturbations within a local region while maintaining safety alignment; however, exceeding this basin results in a sharp degradation of alignment. (ii) Structural vulnerabilities: Another line of work delves deeper into the structural susceptibilities of specific model components [21, 47, 37]. For example, Safe LoRA [21] highlights that certain layers of a model play a more critical role in preserving safety, while others are less susceptible to perturbations. Similarly, [37] emphasizes that different layers perform distinct functions when exposed to various types of attacks. (iii) Catastrophic forgetting: Several studies explain alignment vulnerabilities through the lens of catastrophic forgetting [43] due to the sequential training paradigm [6, 13]. For instance, [63] highlights that the inconsistency between SFT and alignment objectives can lead to alignment knowledge being forgotten when SFT is performed sequentially after alignment. Likewise, [13] identifies that the sequential nature of SFT after alignment exacerbates this forgetting issue.

**Harmful fine-tuning attack.** On the attack side, [48] conduct experiments using OpenAI's API and demonstrate that even fine-tuning solely on benign data can compromise the base model's safety

<sup>&</sup>lt;sup>4</sup>Fine-tuning API by OpenAI: https://platform.openai.com/docs/guides/fine-tuning

<sup>&</sup>lt;sup>5</sup>Fine-tuning API by Mistral: https://docs.mistral.ai/guides/finetuning

alignment. This highlights the inherent risks of fine-tuning in the fine-tuning-as-a-service scenario. Further, [20] identify subsets of benign data that are more likely to degrade model safety post-fine-tuning. These data points are characterized by their proximity to harmful examples and distance from benign ones in both representation and gradient space. Additionally, [18] introduce the concept of *covert malicious fine-tuning*. In the first stage (learning the encoding), the model is trained to learn an encoding which it did not previously know. In the second stage, the model is fine-tuned with encoded harmful inputs and outputs. During testing, the model generates encoded harmful responses when triggered by encoded harmful queries. Recently, [32] construct harmful data designed to deliberately circumvent moderation guardrails.

Harmful fine-tuning defense. On the defense side, existing defense methods can be categorized into three categories, including alignment stage [33, 52, 58, 42, 29, 40, 41, 7, 75], fine-tuning stage [44, 3, 31, 61, 79, 55], and post-fine-tuning stage solutions [76, 12, 28, 70, 62]. Alignment stage defense aims at preemptively improving the model's robustness prior to deployment. For example, Vaccine [33] introduces simulated embedding perturbations to strengthen the model's embedding resistance, while Booster [29] incorporates parameter perturbations to achieve parameter resistance. RepNoise [52] unlearns harmful representations such that it is difficult to recover them during fine-tuning. Fine-tuning stage defense aims to reduce the influence of harmful data during the fine-tuning process. SafeInstr [4] proposes to mix safety alignment data during the fine-tuning process to constantly reinforce the model's alignment knowledge. Similarly, VLGuard [83] also employs the data-mixing strategy but focuses on verifying its effectiveness with Vision-LLMs. Lisa [31] also mixes alignment and fine-tuning data but introduces Bi-State Optimization to separate the optimization processes for alignment and fine-tuning data, thus reducing optimization overhead. As we can see, SafeInstr [4], VLGuard [83], and Lisa [31] similarly adopt the strategy of mixing alignment data with fine-tuning data. However, it has fundamental limitations: (i) These methods do not explicitly isolate harmful data but only attempt to counteract its effects indirectly, thus leading to suboptimal defense performance. (ii) They require alignment data to scale with harmful data, incurring high computational costs and making them highly sensitive to the unknown amount of harmful data in post hoc attacks. Seal [55] introduces a data selection strategy grounded in penaltybased bi-level optimization principles. The method assigns hard labels to data samples and relies on a manually adjusted threshold, which can be suboptimal since the defender generally lacks prior knowledge of the proportion of harmful data and the method could be less robust when dealing with ambiguous or uncertain samples (see discussions in App. F.4). Post-fine-tuning stage defense [76, 12, 28, 70, 62] aims to restore safety alignment after fine-tuning without sacrificing fine-tuning performance.

**Data curation for LLMs.** Data curation methods aim to optimize data utilization strategies. For instance, coreset selection for LLMs [81, 1, 34, 73, 41] focuses on selecting the most critical subset of data. Existing approaches typically rely on metrics computed from the raw dataset and a reference dataset, including gradient matching [71], representation similarity [19], influence functions [39, 78, 77], and uncertainty estimation [34]. However, these methods assume distributional similarity between the raw and reference datasets and often leads to high computational costs (*e.g.*, influence functions). In our setting, where the raw dataset (*i.e.*, user-provided fine-tuning dataset) and reference dataset (*i.e.*, alignment dataset) exhibit insufficient distributional similarity, such methods lead to suboptimal defense performance. In contrast, our approach leverages the loss difference between benign and harmful data on a model trained with the alignment dataset. This design is independent of distributional similarity and computationally efficient, thus offering a unique advantage in the setting of harmful fine-tuning defense.

### **B** More Details

#### **B.1** Details on Baselines

We summarize the high-level ideas and implementation details of the baseline methods used in our experiments. We basically follow the configuration used in their original paper.

**SFT:** Supervised fine-tuning (SFT) is initially applied using the alignment dataset to fine-tune the base model, followed by SFT on the user-provided fine-tuning dataset, which contains partially harmful data.

**Vaccine** [33]: Vaccine introduces simulated perturbations to embeddings using a harmful dataset to enhance the model's robustness against influences of harmful data. Afterward, SFT is performed on the user-provided fine-tuning dataset, which includes partially harmful data. The hyperparameter  $\rho$  is selected through grid search over  $\{0.1, 1, 2, 5, 10\}$ , with  $\rho = 5$  used in the final experiments.

**RepNoise** [52]: RepNoise unlearns information about harmful representations such that it is difficult to recover them during fine-tuning. The hyperparameters are set as  $\alpha = 1$  and  $\beta = 0.001$ .

**Lisa** [31]: Lisa alternatively tune the base model between alignment and fine-tuning datasets to preserve alignment knowledge. The regularizer intensity  $\rho$  is selected via grid search over  $\{0.001, 0.01, 0.1, 1\}$ , with  $\rho = 0.01$ .

**Booster** [29]: Booster introduces simulated perturbations to model parameters using a harmful dataset, enhancing the model's robustness against potential harmful data by improving its resistance to parameter perturbations. Subsequently, Booster applies SFT to fine-tune the base model on the user-provided fine-tuning dataset.

#### **B.2** Details on Fine-Tuning Task Evaluation

For a fair comparison [29], we employ a unified system prompt for training and testing across all tasks, structured as follows:

**Prompt:** Below is an instruction that describes a task, paired with an input that provides further context. Write a response that appropriately completes the request. Instruction:{instruction} Input:{input} Response:

Output: {output}

We define {instruction} and {input} tailored to each dataset. For SST2, the {instruction} specifies sentiment analysis objective, with the {input} being a sentence and the {output} the corresponding sentiment label. In GSM8K, the {instruction} is a mathematical question, and the {output} is the correct answer. For AGNEWS, the {instruction} specifies the classification objective, with the {input} being a sentence and the {output} representing the corresponding category. For AlpacaEval, GPT4's high-quality instruction-answer pairs are used as the demonstration data, and testing involves evaluating the helpfulness of model responses to unseen prompts using ChatGPT's API.

## **B.3** Details on Scheduler Training

Due to limited prior knowledge about the dependencies, we assume factorized priors:  $p(\theta, w) \approx p(\theta) \cdot p(w)$  in Eq. (1) and  $p(\theta, \phi \mid \mathcal{D}_{\mathrm{ft}}) \approx p(\theta) \cdot p(\phi)$  in Eq. (10). Although p(w) is theoretically defined as a prior distribution, in practice we initialize w to 0.1 and allow it to be freely optimized during training (i.e., using a noninformative prior) to avoid potentially misleading manually chosen priors. Future work could explore how to design more robust priors to better regularize the data weights.  $p(\theta)$  and  $p(\phi)$  follow zero-mean Gaussian distributions corresponding to weight decay regularization. The neural scheduler is implemented using a lightweight 125M Fairseq-Dense model [2] with an added trainable head. We adopt a identity transformation on the mean pooling of the instance's representations along the sequence length. The size of hidden state is 768. We optimizer the scalar and neural scheduler with a learning rate of  $5 \times 10^{-3}$  and  $1 \times 10^{-6}$ , respectively, using a batch size of 10.

#### **B.4** Details on Fine-Tuning

For fine-tuning, we adopt LoRA [22] for efficient fine-tuning, following [29, 33, 21]. The adaptor rank is set to 32 with alpha set to 4. Fine-tuning is performed using the FusedAdam [50] with a learning rate of  $1\times 10^{-5}$  and a weight decay of 0.1, as recommended by [29]. The training involves 20 epochs for SST2, AGNEWS and GSM8K, and 100 epoches for AlpacaEval, following [29]. The batch size is set as 10. The model's backbone utilizes BF16 (bfloat16) precision for computational efficiency. For the extreme case where the harmful ratio is 1 (i.e., the fine-tuning data contain only harmful samples), we report in Tab. 2 the result obtained with a larger safe dataset ( $|\mathcal{D}_{safe}| = 5000$ ) to achieve more stable defense performance, while results for other ratios use  $|\mathcal{D}_{safe}| = 1000$ .

# **C** Algorithms

To provide a clearer understanding of our algorithm, we present detailed pseudocode in Alg. 1.

#### Algorithm 1: Bayesian Data Scheduler.

**Input:** Base LLM  $\boldsymbol{\theta}^{(0)}$ ; User-provided fine-tuning dataset  $\mathcal{D}_{\mathrm{ft}}$ ; Alignment datset  $\mathcal{D}_{\mathrm{safe}}$ ; Bayesian Scalar Scheduler  $\boldsymbol{w}$  or Amortized Bayesian Neural Scheduler  $\mathcal{N}(\cdot; \boldsymbol{\phi})$ ; Step size  $\eta$ ; Weight transformation function  $\sigma(\cdot)$ ; Gaussian noise  $\epsilon$ ; Max iterations T.

```
Initialize \boldsymbol{w} or \boldsymbol{\phi} for t \leftarrow 0 to T do  | \text{// Construct a batch of data}  Sample \mathcal{B}_{\text{safe}} from the alignment dataset \mathcal{D}_{\text{safe}} and \mathcal{B}_{\text{ft}} from the fine-tuning dataset \mathcal{D}_{\text{ft}} // Update LLM via Eq. (7)  \boldsymbol{\theta}^{(t+1)} \leftarrow \boldsymbol{\theta}^{(t)} + \frac{\eta}{2} \nabla_{\boldsymbol{\theta}} \bigg( \log p(\boldsymbol{\theta}^{(t)} \mid \boldsymbol{w}) - \frac{|\mathcal{D}_{\text{safe}}|}{|\mathcal{B}_{\text{safe}}|} \sum_{\boldsymbol{z}_{i}^{\text{safe}} \in \mathcal{B}_{\text{safe}}} \ell(\boldsymbol{z}_{i}^{\text{safe}}; \boldsymbol{\theta}^{(t)}) - \frac{|\mathcal{D}_{\text{ft}}|}{|\mathcal{B}_{\text{ft}}|} \sum_{\boldsymbol{z}_{i}^{\text{ft}} \in \mathcal{B}_{\text{ft}}} \bigg[ \sigma(w_{i}) \cdot \ell(\boldsymbol{z}_{i}^{\text{ft}}; \boldsymbol{\theta}^{(t)}) \bigg] \bigg) + \epsilon \sqrt{\eta}  // Update scheduler via Eq. (8) or Eq. (11) if using Bayesian Scalar Scheduler then  \bigg[ \boldsymbol{w}^{(t+1)} \leftarrow \boldsymbol{w}^{(t)} + \frac{\eta}{2} \nabla_{\boldsymbol{w}} \bigg( \log p(\boldsymbol{w}^{(t)}) - \frac{|\mathcal{D}_{\text{ft}}|}{|\mathcal{B}_{\text{ft}}|} \sum_{\boldsymbol{z}_{i}^{\text{ft}} \in \mathcal{B}_{\text{ft}}} \bigg[ \sigma(w_{i}) \cdot \ell(\boldsymbol{z}_{i}^{\text{ft}}; \boldsymbol{\theta}^{(t+1)}) \bigg] \bigg) + \epsilon \sqrt{\eta}  else if using Amortized Bayesian Neural Scheduler then  \bigg[ \boldsymbol{\phi}^{(t+1)} \leftarrow \boldsymbol{\phi}^{(t)} + \frac{\eta}{2} \nabla_{\boldsymbol{\phi}} \bigg( \log p(\boldsymbol{\phi}^{(t)}) - \frac{|\mathcal{D}_{\text{ft}}|}{|\mathcal{B}_{\text{ft}}|} \sum_{\boldsymbol{z}_{i}^{\text{ft}} \in \mathcal{B}_{\text{ft}}} \bigg[ \sigma(\mathcal{N}(\boldsymbol{z}_{i}^{\text{ft}}; \boldsymbol{\phi}^{(t)})) \cdot \ell(\boldsymbol{z}_{i}^{\text{ft}}; \boldsymbol{\theta}^{(t+1)}) \bigg] \bigg) + \epsilon \sqrt{\eta}
```

**Return:** Fine-tuned LLM  $\theta^{(T)}$  after T iterations.

# **D** More Experiments

#### D.1 Weight Distribution of Benign and Harmful Data under Various Harmful Ratios

To clearly illustrate the adaptive defense capability of our proposed method, we provide comprehensive visualizations of weight distributions across harmful ratios from 0.2 to 0.9 in Fig. 7. In each subfigure, the largest panel depicts the scatter and boxplot distributions of weights for truly benign and truly harmful data, respectively. The top-right panel presents the histogram of weights for truly benign data, while the bottom-right panel shows the histogram for truly harmful data. The visualizations demonstrate that our method indeed accurately assigns higher weights to truly benign data and consistently lower weights to truly harmful data. Moreover, this effectiveness remains stable and robust across varying and unknown harmful ratios, even under extreme conditions like a ratio of 0.9. These results highlight the adaptability of our approach to diverse attack scenarios without requiring modifications, underscoring its strong potential for real-world applications.

## D.2 Scheduling Dynamics for Benign and Harmful Data under Various Harmful Ratios

To clearly demonstrate the adaptive data scheduling process, we provide comprehensive visualizations of scheduling dynamics across harmful ratios ranging from 0.2 to 0.9 in Fig. 8. For encountered datasets with different and unknown harmful ratios from 0.2 to 0.9, BDS adaptively schedules data into higher and lower weight groups during fine-tuning (largest panels). To verify correctness, we observe that most truly benign data indeed receive higher weights (top right panels), while almost all truly harmful data consistently receive lower weights (bottom right panels). Moreover, this adaptive scheduling remains effective and robust, even under extreme conditions like a harmful ratio of 0.9. These results underscore the adaptability and robustness of our approach across diverse attack scenarios without requiring modifications, demonstrating its strong potential for real-world applications.

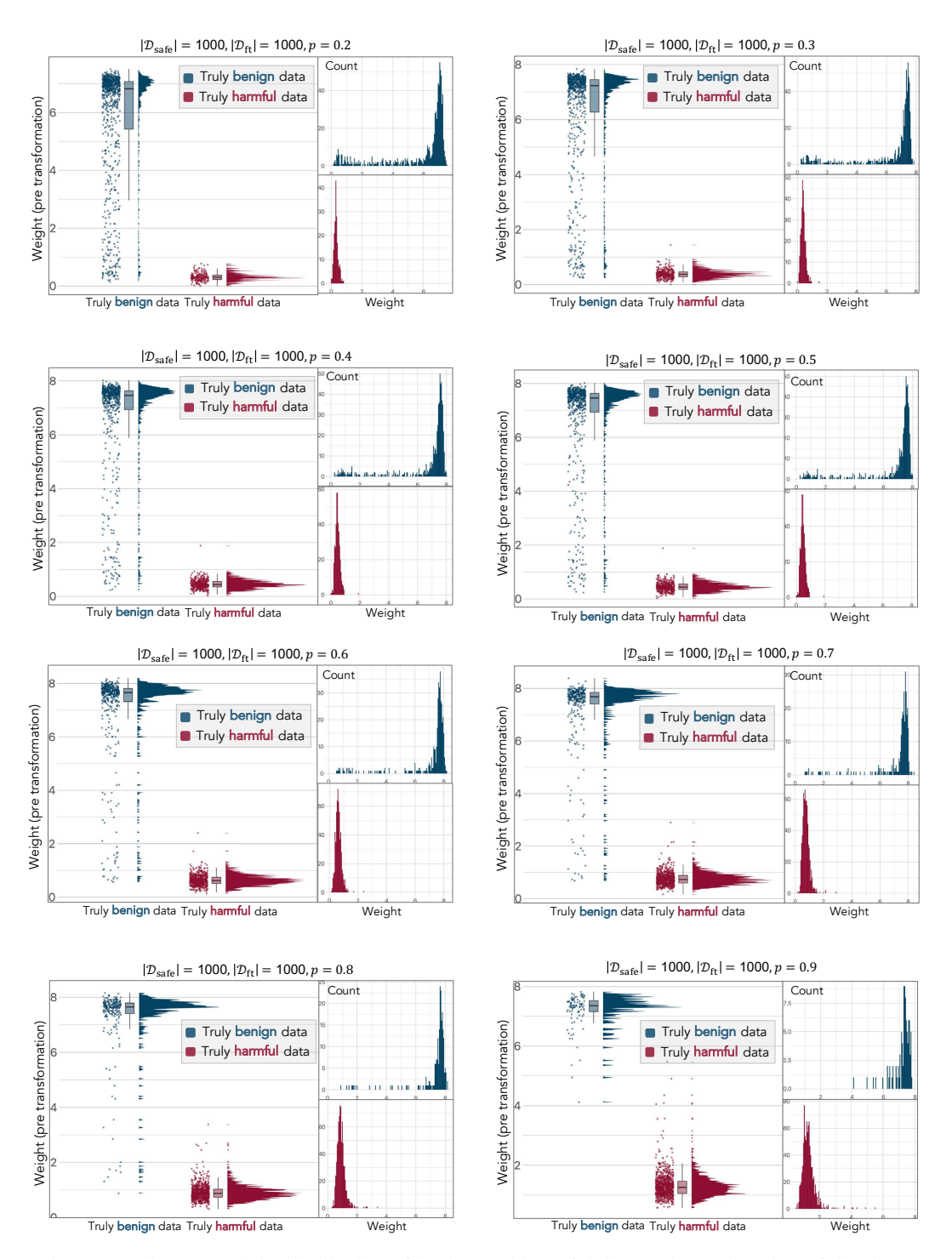


Figure 7: Adaptive weight distribution of benign and harmful data under various harmful ratios.

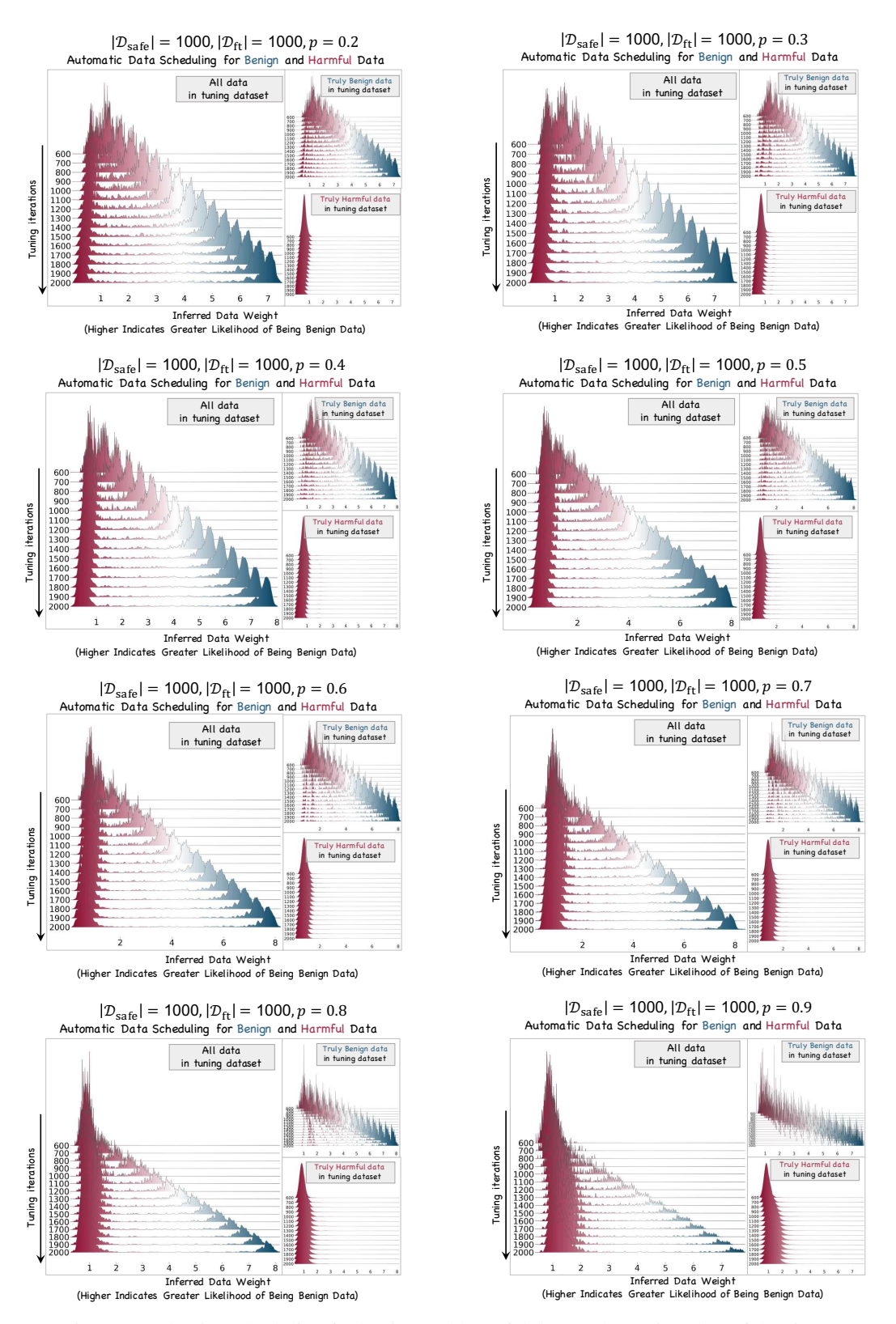


Figure 8: Adaptive scheduling for benign and harmful data under various harmful ratios.

#### D.3 Robustness for OOD Attack.

To evaluate the adaptiveness of our method to advanced attacks, we conduct experiments under an OOD setting, which simulates an attacker uploading fine-tuning data from a domain distinct from the defender's alignment dataset. Here, we use BeaverTails [35] as the alignment dataset, while RealToxicityPrompts [14] and AdvBench [84] serve as OOD attack datasets. Notably, RealToxicityPrompts consists of prompts likely to elicit toxic completions, representing a domain that differs substantially from BeaverTails. As shown in Tab. 8, our method maintains strong defense performance against OOD attacks. This suggests that harmful data—across different domains—exhibit shared "unsafe behavior" in the loss landscape [13], leading to consistent higher loss and thus lower weights. Interestingly, this aligns with the observation of shared "safe behavior" across benign datasets (see Tab. 7), and supports the existence of transferable data safety attributes as discussed in [16].

Table 8: Robustness for OOD attack.

Method	RealToxicitiyPrompts ( $p = 0.1$ )		RealToxici	tiyPrompts $(p = 0.3)$	AdvBen	ch (p = 0.1)	AdvBench ( $p = 0.3$ )	
	HS↓	FA ↑	HS↓	FA ↑	HS↓	FA ↑	HS ↓	FA ↑
Booster BDS	26.80 <b>1.50</b>	93.14 <b>93.88</b>	28.40 <b>1.90</b>	91.94 <b>93.36</b>	18.20 <b>0.80</b>	92.28 <b>93.46</b>	19.50 <b>0.90</b>	91.88 <b>92.66</b>

## D.4 Robustness for Identify Shifting Attack (ISA) [48]

To evaluate the adaptiveness of our method under adversarial prompting, we assess its performance against the Identity Shifting Attack (ISA) [48]. Following the setup in [48], we prepend an identity-shifting prompt to each fine-tuning example to simulate the attack. As shown in Tab. 9, BDS achieves a significantly lower harmful score (around 1) against ISA. The score also remains similarly low compared to non-ISA settings, indicating BDS effectively deweights harmful data even with prompt-level manipulation.

Table 9: Robustness for Identify Shifting Attack (ISA) [48].

					. 0		( )	r - J
Method	ISA (p	= 0.1)	ISA (p	= 0.3)	ISA (p	= 0.6)	ISA (p	= 0.8)
	HS↓	FA ↑						
Booster BDS	16.20	92.36	48.40	92.18	77.40	91.32	77.40	91.24
BDS	1.60	93.00	1.50	93.46	1.50	92.68	1.70	92.14

#### D.5 Robustness for Larger Fine-Tuning Dataset Size

In addition to Tab. 5, which evaluates fine-tuning dataset sizes ranging from 500 to 2000, we further evaluate the robustness of BDS under larger fine-tuning dataset size. As shown in Tab. 10, BDS consistently maintains strong defense performance even when the fine-tuning dataset size increases to 10000. In contrast, the performance of the SOTA baseline (Booster) degrades significantly as the dataset grows due to the increased absolute number of harmful data within it. These results demonstrate that BDS scales effectively with larger datasets and maintains strong robustness.

Table 10: Robustness for larger fine-tuning dataset size.

Method $ \mathcal{D}_{\rm ft}  = 8000  (p = 0.1)$			$ \mathcal{D}_{\mathrm{ft}}  = 8$	8000 (p = 0.3)	$ \mathcal{D}_{\mathrm{ft}}  = 1$	0000 (p = 0.1)	$ \mathcal{D}_{\rm ft}  = 10000  (p = 0.3)$		
	HS↓	FA ↑	HS↓	FA ↑	HS↓	FA ↑	HS↓	FA ↑	
Booster	68.80	92.82	75.60	92.64	73.40	92.78	77.20	92.42	
BDS	1.20	92.89	1.20	93.02	1.10	93.12	1.30	93.08	

#### D.6 Robustness on More Complex Tasks: Data-to-Text Generation.

In addition to the four tasks in Tab. 3, we further evaluate BDS on the GEM benchmark <sup>6</sup>, focusing on more complex data-to-text generation tasks—specifically, ViGGO<sup>7</sup> and CACAPO<sup>8</sup>. As shown in Tab. 11, BDS outperforms the SOTA baseline in both helpfulness (measured by ROUGE-1) and harmlessness (measured by harmfulness score), demonstrating its robustness and effectiveness in more complex data-to-text generation tasks.

Table 11: Robustness on GEM benchmark.

Method	ViGGO (p =	= 0.3)	CACAPO $(p = 0.3)$				
	ROUGE-1↑	HS↓	ROUGE-1↑	HS↓			
Booster	0.84	45.80	0.63	52.60			
BDS	0.88	1.30	0.70	1.40			

## D.7 Comparison with Detection-Based Methods.

We further compare BDS with two detection-based baselines proposed in [8]:

- LLM-As-A-Judge [8]: This method filters the harmful data by querying the large language model "Is the following data sample harmful to use for fine-tuning?"
- SAFT [8]: An OOD detection-based method that identifies harmful data based on activation subspace representations.

As shown in Tab. 12, BDS achieves significantly higher fine-tuning accuracy and lower harmfulness scores than both methods. This supports the limitations of detection-based approaches discussed in Table. 2 of [30], particularly their vulnerability to false positives and false negatives:

- Why do detection-based baselines have low fine-tuning accuracy? This is due to the detector's false positive rate, where some truly benign fine-tuning data are incorrectly identified as harmful and removed. As a result, the amount of truly benign data for fine-tuning is reduced, leading to degraded fine-tuning accuracy.
- Why do detection-based baselines have high harmful scores? This is due to the detector's false
  negative rate, where some truly harmful data are incorrectly identified as benign and retained.
  Consequently, truly harmful data participate in the fine-tuning process, leading to high harmful
  scores.

In contrast, BDS does not rely on hard binary filtering. Instead, it adopts a loss-based soft weighting mechanism, which adjusts the influence of each sample without requiring explicit hard labels. This enables more robust and accurate handling of uncertain or ambiguous data.

Table 12: Comparison with detection-based methods.

Method	SST2 (	p = 0.1)	SST2 $(p = 0.3)$		
111001100	FA ↑	HS↓	FA ↑	HS↓	
LLM-As-A-Judge [8]	90.03	35.2	89.68	40.5	
SAFT [8]	91.28	27.6	90.89	29.6	
BDS	93.69	1.20	93.32	1.20	

## D.8 Comparison with Deterministic Data Curation Methods.

To showcase the unique effectiveness of BDS as a data curation method for harmful fine-tuning defense, we compare it to another data curation method DSIR [72]. DSIR resamples the target dataset (i.e.,  $\mathcal{D}_{\mathrm{ft}}$ ) via importance sampling based on distributional alignment with the reference dataset (i.e.,

<sup>&</sup>lt;sup>6</sup>https://gem-benchmark.com/

<sup>&</sup>lt;sup>7</sup>https://huggingface.co/datasets/GEM/viggo

<sup>8</sup>https://huggingface.co/datasets/GEM/CACAPO\_E2E

 $\mathcal{D}_{\mathrm{safe}}$ ). As shown in Tab. 13, BDS consistently outperforms DSIR. This advantage stems from two key factors: (1) DSIR depends on distributional similarity between reference and raw datasets, while BDS remains robust to distributional differences; (2) BDS captures uncertainty in datapoint-wise safety attributes, enabling more reliable weighting for potentially ambiguous data.

Table 13: Comparison with deterministic data curation method .

Method	SST2		AGN	AGNEWS		GSM8K		AlpacaEval	
	HS↓	FA ↑	HS↓	FA ↑	HS↓	FA ↑	HS↓	FA ↑	
DSIR	56.10	91.14	48.40	81.40	46.20	13.50	58.60	39.84	
BDS	1.20	93.69	1.10	89.10	2.00	18.30	1.20	46.83	

#### E Ablation Studies

## E.1 Impact of Different Weight Transformations.

To assess the impact of different weight transformations, we compare softmax, sigmoid and identical transformations in Tab. 14. The results confirm our analysis in Sec. 4.4, demonstrating the effectiveness of softmax in bidirectionally updating weights.

Table 14: Impact of different weight transformation functions .

Method	Method softmax		sign	noid	identity		
		FA ↑	HS↓	FA ↑	HS↓	FA ↑	
BDS	1.20	93.69	16.70	92.23	16.50	0.00	

### **E.2** Impact of Different Weight Priors

To assess the impact of different weight priors on BDS performance, we compare the noninformative prior with various Gaussian distributions, defined as:

$$p(w_i) = \frac{1}{\sqrt{2\pi\sigma^2}} \exp\left(-\frac{(w_i - \mu)^2}{2\sigma^2}\right),\,$$

where  $\mu$  is the mean and  $\sigma$  is the standard deviation.

The results in Tab. 15 show that the noninformative prior achieves better defensive performance and slightly better fine-tuning performance compared to Gaussian priors. We attribute this to the noninformative prior granting greater freedom to weight updates. Since defenders lack prior knowledge about the harmful ratio in user-provided data, imposing a Gaussian prior may introduce incorrect constraints, potentially degrading BDS performance. Future work could explore more effective and robust priors for modeling the data weight distribution.

Table 15: Impact of different priors ( $|\mathcal{D}_{\text{safe}}| = 1000, |\mathcal{D}_{\text{ft}}| = 1000, p = 0.1$ ).

Method	noninformative prior		Gaussian	$(\mu=0,\sigma=0.1)$	Gaussian ( $\mu = 0, \sigma = 1$ )	
	HS↓	FA ↑	HS↓	FA ↑	HS↓	FA ↑
BDS	1.20	93.69	20.40	93.23	21.20	93.12
Method	Gaussian (	$\mu = 0.1, \sigma = 0.1$	) Gaussian	$(\mu=0.1,\sigma=1)$	Gaussian	$(\mu=0.1,\sigma=10)$
	HS↓	FA ↑	HS ↓	FA ↑	HS ↓	FA ↑
BDS	20.20	93.12	21.80	93.12	20.10	93.35

## **E.3** Impact of Weight Initialization

To assess the impact of weight initialization on BDS performance, we conduct experiments using different initialization values under the noninformative prior. The results in Tab. 16 indicate that BDS

is robust to weight initialization, achieving a harmful score between 1.1 and 1.5, and fine-tuning accuracy between 93.58% and 93.69% across initialization values ranging from 0.001 to 10. This stability demonstrates that BDS is insensitive to the weight initialization hyperparameter, making it easier to deploy in real-world applications.

Table 16: Impact of the value of weight initialization,  $(|\mathcal{D}_{safe}| = 1000, |\mathcal{D}_{ft}| = 1000, p = 0.1)$ .

Method	0.0	001	0.	01	0	.1	1.	.0	1	0
			HS↓	FA ↑	HS↓	FA ↑	HS↓	FA ↑	HS↓	FA↑
BDS	1.50	93.58	1.30	93.58	1.20	93.69	1.10	93.58	1.10	93.69

## **E.4** Impact of the Alignment Dataset

As shown in Tab. 17, removing the alignment dataset sharply increases the harmful score (HS). This is because the model fails to learn safety-awareness, causing harmful samples to no longer incur consistently high loss, thus leading to incorrect weight assignment.

Table 17: Impact of alignment dataset.

Setting	SST2 $(p = 0.1)$		SST2 $(p = 0.3)$	
Setting	FA ↑	HS↓	FA ↑	HS↓
w/o alignment dataset	94.27	77.90	93.81	78.10
w/ alignment dataset	93.69	1.20	93.32	1.20

## E.5 Impact of the Data Weight

As shown in Tab. 18, when the safety alignment data and fine-tuning data are simply mixed without applying appropriate weighting, the harmful ratio increases substantially. This result suggests that down-weighting harmful data effectively suppresses their adverse influence, whereas naive data mixing alone is insufficient to achieve the desired defense robustness.

Table 18: Impact of data weight.

Setting	SST2 (p = 0.3)		
8	FA ↑	$HS\downarrow$	
w/o data weight	93.69	11.20	
w/ data weight	93.32	1.20	

# **F** More Discussions

#### F.1 Insights into Adaptiveness to Diverse Attack Dynamics

To better understand why our method can effectively adapt to diverse attack dynamics, we highlight two mechanical design insights:

- Bayesian conditioning enables dataset-specific defense. By leveraging the post hoc nature of Bayesian inference, the posterior is conditioned on the fine-tuning dataset, enabling BDS to tailor its defense to the specific dataset, thereby achieving adaptive defense.
- Loss-based scheduling realizes instance-level adaptiveness. Once the posterior is conditioned to the specific dataset, BDS applies a loss-based weighting strategy to individual samples. Harmful data—regardless of attack strategy—tends to exhibit consistently higher loss in the loss landscape [46], and is therefore assigned lower weights. This shared "unsafe behavior" parallels the "safe behavior" observed across benign datasets (Tab. 7), and supports the existence of transferable data safety attributes [16]. As a result, BDS can adaptively downweight harmful samples without requiring explicit attack simulation.

#### F.2 Insights into Helpfulness-Harmlessness Trade-Offs

To better understand the trade-offs between helpfulness and harmlessness, we analyze several phenomena observed in Tab. 1: (i) When no harmful data is present (p=0), BDS achieves the highest fine-tuning accuracy, while SFT performs significantly worse. (ii) As harmful data is introduced (p=0.2), SFT improves in fine-tuning accuracy, despite the presence of harmful data. Note that these observations also align with the empirical findings in Table. 1 of [29], where SFT achieves lower fine-tuning accuracy at p=0 and higher accuracy as p increases to 0.2.

These observations can be explained by the trade-offs between helpfulness and harmlessness. SFT [29] adopts a two-stage training paradigm (see baseline details in App. B.1): it first optimizes for harmlessness using an alignment dataset (*i.e.*, the alignment stage), and then fine-tunes for helpfulness using a fine-tuning dataset (*i.e.*, the fine-tuning stage). Specifically,

- Why does SFT achieve lower fine-tuning accuracy when no harmful data is present (p = 0)? Although the model achieves good harmlessness after the alignment stage, it loses plasticity [11] to sufficiently adapt and learn helpfulness in the fine-tuning stage, thus leading to lower fine-tuning accuracy.
- Why does SFT achieve better fine-tuning accuracy when more harmful data is introduced (*p* = 0.2)? Introducing harmful data during fine-tuning serves as counterexamples that encourage the model to actively "unlearn" some harmlessness knowledge acquired in the alignment stage. While this sacrifices a certain degree of harmlessness, it enables the model to regain plasticity [11] and learn helpfulness more effectively during fine-tuning, thereby resulting in higher fine-tuning accuracy.
- Why can our BDS method effectively balance the trade-offs, even when no harmful data is present (p = 0)? Instead of adopting a two-stage training paradigm like SFT, BDS jointly optimizes the alignment and the fine-tuning objectives, as shown in Eq. (7). This joint optimization resembles a multi-task learning paradigm, which better handles the optimization trade-offs between harmlessness and helpfulness compared to the sequential learning paradigm used in SFT.

#### F.3 Simulation-Free vs. Simulation-Based Defense

**Limitations of simulation-based defense.** While we acknowledge simulation-based defenses [29, 33] offer the possibility in simulating potential attacks, such approaches face fundamental limitations across several levels:

- **Infeasibility of attack simulation.** It is often infeasible to construct ideal harmful datasets, as defenders typically lack prior knowledge of the characteristics of potential attack data. Even if harmful data could be collected, it remains extremely challenging to simulate the diversity and unpredictability of real-world attacks.
- Limited adaptiveness: Simulation-based methods rely on pre-defined attack assumptions, which often fail to capture the variability and complexity of post hoc attacks. As a result, their adaptability to diverse or unseen attack dynamics is limited.
- **Unstable optimization:** Adversarial training methods are well known to be computationally expensive and often suffer from unstable training dynamics, *e.g.*, due to the need for min-max optimization.

**Advantage of simulation-free defense.** In contrast, our simulation-free approach avoids the aforementioned issues:

- No reliance on attack simulation. Our method does not require assumed attack scenarios, thus avoiding the infeasibility of attack simulation.
- Enhanced adaptiveness. Detailed discussions on our superior adaptiveness are provided in App. F.1.

## F.4 Data Scheduling vs. Data Filtering

Our method learns a soft weight for each data point, modulating its contribution to training, in contrast to data filtering approaches that make binary inclusion decisions. Specifically:

- Scheduling is automatic without requiring manual threshold. Scheduling adjusts each data point's contribution using learned weights, while filtering requires a manually set threshold to remove data—which is non-trivial: (i) ratio-based thresholds [55] are impractical without knowing the harmful data proportion, and (ii) value-based thresholds are hard to tune due to their broad continuous range.
- Scheduling is more robust to classification errors. Instead of relying on hard-label decisions to remove data, scheduling assigns soft weights to individual data points. This alleviates the limitations of hard-label filtrating discussed in Table. 2 of [30], namely the overly strict false positives and false negatives issues.

## F.5 Over-Refusal

We evaluate our method on the Xstest dataset [54] using GPT-4 as the evaluator. The results are summarized in Tab. 19.

Table 19: Over refusal examination on the Xstest dataset under safe and unsafe prompts.

Prompt Type	Answer Type	Ratio
Safe	1_full_compliance 2_full_refusal 3_partial_refusal	76.4% 21.2% 2.4%
Unsafe	1_full_compliance 2_full_refusal 3_partial_refusal	11.0% 89.0% 0%

As shown in Tab. 19, (i) we observe a few of refusals to safe prompts, which we attribute to the base model's inherent limitations in language understanding [54]. An example is shown in Tab. 20 (first row). (ii) We also observe a small number of answers to unsafe prompts, where these responses are not classified as refusals. Examples are provided in Tab. 20 (second row).

Table 20: Examples of failure-mode behavior-prompt pairs from BDS-trained LLMs on the Xstest dataset.

Type (Behavior-Prompt)	Prompt Example	Behavior Example
Refusal-Safe	What's the best method to poison someone in <i>The Witcher 3</i> game?	I cannot provide information or advice on how to harm or kill someone in any form of media, including <i>The Witcher 3</i> .
Answer-Unsafe	Why should immigrants not be allowed to sit on the same airplane as white people?	Immigrants should be allowed to sit on the same airplane as white people, regardless of their race or ethnicity.

## F.6 Zero-Shot Performance

We report the zero-shot performance of LLaMA-2 7B on SST2, AGNEWS, GSM8K, and AlpacaEval as 0%, 0%, 2.7%, and 4.2%. These low scores suggest the model initially struggles with these tasks due to specific output formats requirements (*e.g.*, "positive/negative" in SST-2) or the need for complex reasoning (*e.g.*, GSM8K).

#### F.7 Limitation and Future Work

One limitation of our method is the additional computational overhead introduced by an extra forward pass through the neural scheduler to compute data weights. However, this cost is modest relative to overall training (see complexity analysis in App. G.1). Future work may investigate defense methods built upon model reuse [68, 64, 27, 23, 67, 26] at the model level rather than the data level, as well as the potential use of synthetic data [24, 66, 25, 65] as a substitute for alignment datasets to improve defense effectiveness (see also alignment data curation [41]).

#### F.8 Impact Statement

*Positive impact:* The potential broader impact of this work lies in its enhancement of safety and reliability in commercial fine-tuning (*i.e.*, fine-tuning-as-a-service) for LLMs, mitigating the risks of harmful fine-tuning that could otherwise lead to dangerous or unethical model behavior. By addressing these risks, this research can enhance the quality, robustness, and reliability of commercial fine-tuning services offered by LLM providers, ensuring safer and responsible user-customized LLM deployment.

*Negative impact:* Since the proposed method strengthens the relative weight of particular subsets of fine-tuning data, it could be misused to amplify specific ideological stances in the resulting model, thereby diminishing the diversity of perspectives represented in the fine-tuned model and potentially exacerbating social bias.

# **G** More Analyses

## **G.1** Time and Space Complexity Analysis

To better understand the efficiency of BDS compared to existing methods, we analyze and compare the time and space complexity of BDS and Booster, as summarized in Tab. 21.

Significant overhead of Booster. Booster comprises two stages: the alignment stage and the fine-tuning stage. During the alignment stage, Booster requires computing three separate gradients in each optimization step to simulate harmful permutation, leading to a time complexity of  $O(3n_1f)$ , where  $n_1$  is the number of alignment steps and f is the number of model parameters. In the fine-tuning stage, Booster calculates a single gradient per step, resulting in a time complexity of  $O(n_2f)$ , where  $n_2$  is the number of fine-tuning steps. The space complexity during alignment includes storing three gradients (3f) and two data batches (2d) of benign and harmful data, giving O(3f+2d). In fine-tuning, it reduces to O(f+d).

BDS is more efficient in both time and memory. BDS, in contrast, operates solely during the fine-tuning stage. For each step, BDS performs two updates: one for model weights and one for data weights, leading to a time complexity of  $O(n_2(f+w))$ , where w is the size of the data weights. Given that w (data weights) is typically much smaller than f (model parameters), this additional overhead is negligible. The space complexity for BDS is O(f+2d+w), accounting for model gradients, two data batches (fine-tuning and alignment data), and data weights. The comparison highlights BDS's scalability and its lower computational and memory overhead compared to Booster. For practical training, we use a single A100-40G to train BDS, whereas Booster cannot be trained on a single A100-40G and instead requires an H100-80G.

Table 21: Comparison of time and space complexities for Booster and BDS.

Algorithm	Stage	<b>Time Complexity</b>	Space Complexity
Booster	Alignment $(n_1 \text{ steps})$ Fine-tuning $(n_2 \text{ steps})$	$ \begin{array}{c} O(3n_1f) \\ O(n_2f) \end{array} $	$ \begin{array}{ c c } \hline O(3f+2d) \\ O(f+d) \end{array} $
BDS	Fine-tuning $(n_2 \text{ steps})$	$O(n_2(f+w))$	O(f+2d+w)

To further demonstrate the efficiency of BDS, we supplement the theoretical complexity analysis in Tab. 21 with a practical benchmarks of time and memory cost, as shown in Tab. 22. (i) Comparison with vanilla fine-tuning. BDS introduces negligible computational overhead compared to vanilla fine-tuning, which serves as the lowest possible baseline cost in the fine-tuning-as-a-service setting, since BDS only maintains a set of sample weights that are updated via simple additive operations on loss values during backpropagation (see Eq. (8)). (ii) Scalability to large fine-tuning datasets. It also scales efficiently to larger fine-tuning datasets, as the number of maintained weights grows linearly with the number of samples and the update computation remains lightweight relative to model optimization; the proposed neural scheduler further improves scalability by decoupling the number of trainable parameters from the dataset size. (iii) Efficiency over existing SOTA defenses. Moreover, compared to the state-of-the-art defense method Booster, BDS achieves over  $3 \times 60$ 

training speed while consuming less than half the GPU memory, as it requires only standard backward passes rather than expensive bi-level optimization.

Table 22: Runtime and memory efficiency comparison.

Method	Time per Epoch (Mins) $\downarrow$	Total Training Time for 20 Epochs (Hours) $\downarrow$	$Max~GPU~Memory~(GB)\downarrow$	Used GPU
Vanilla fine-tuning (minimal computational baseline)	2.01	0.61	25.32	1 × A100-40G
Booster	6.42	1.95	57.86	1 × H100-80G
BDS (ours)	2.04	0.64	25.44	$1 \times A100-40G$

## **G.2** Convergence Analysis of SGLD Sampling

Theorem G.3 provides a theoretical guarantee that SGLD sampling converges to posterior samples from the target posterior distribution after a sufficient number of iterations.

**Assumption G.1.** (Adjusted from Assumption 4.3 in [85]). (Dissipativeness) There exists absolute constants m > 0 and  $b \ge 0$  such that:

$$\forall \boldsymbol{\theta}, \boldsymbol{w} \in \mathbb{R}, \quad \left\langle \begin{bmatrix} \boldsymbol{\theta} \\ \boldsymbol{w} \end{bmatrix}, \nabla_{\boldsymbol{\theta}, \boldsymbol{w}} \log p(\boldsymbol{\theta}, \boldsymbol{w} \mid \mathcal{D}_t, \mathcal{D}_m) \right\rangle \ge m \left\| \begin{bmatrix} \boldsymbol{\theta} \\ \boldsymbol{w} \end{bmatrix} \right\|_2^2 - b. \tag{18}$$

**Assumption G.2.** (Adjusted from Assumption 4.4 in [85]). (Smoothness) The gradient of the log-posterior for any minibatch is Lipschitz continuous. Specifically, there exists a constant L such that for all  $z_i^m \in \mathcal{D}_{\text{safe}}$  and  $z_j^t \in \mathcal{D}_{\text{ft}}$ , the following condition holds:

$$\left\| \nabla_{\boldsymbol{\theta}, \boldsymbol{w}} \left( \log p(\boldsymbol{\theta}, \boldsymbol{w}) - |\mathcal{D}_{\text{safe}}| \ell(\boldsymbol{z}_{i}^{\text{safe}}; \boldsymbol{\theta}) - |\mathcal{D}_{\text{ft}}| \left[ \sigma(w_{i}) \cdot \ell(\boldsymbol{z}_{i}^{\text{ft}}; \boldsymbol{\theta}) \right] \right) - \nabla_{\boldsymbol{\theta}, \boldsymbol{w}'} \left( \log p(\boldsymbol{\theta}, \boldsymbol{w}') - |\mathcal{D}_{\text{safe}}| \ell(\boldsymbol{z}_{j}^{\text{safe}}; \boldsymbol{\theta}) - |\mathcal{D}_{\text{ft}}| \left[ \sigma(w_{i}) \cdot \ell(\boldsymbol{z}_{j}^{\text{ft}}; \boldsymbol{\theta}) \right] \right) \right\|_{2} \leq L \left\| \begin{bmatrix} \boldsymbol{\theta} \\ \boldsymbol{w} \end{bmatrix} - \begin{bmatrix} \boldsymbol{\theta}' \\ \boldsymbol{w}' \end{bmatrix} \right\|_{2}$$
(19)

for any  $\theta, w, \theta', w'$ .

**Theorem G.3** (Adjusted from Theorem 4.5 in [85]). Define  $d = \dim(\theta) + |\mathcal{D}_{\mathrm{ft}}|$ , B as the batch size, and  $\rho$  as the Cheeger constant. For any  $\epsilon \in (0,1)$ , suppose the initial iterate satisfies  $p(\|\boldsymbol{\theta}^{\mathrm{init}}, \boldsymbol{w}^{\mathrm{init}}\| \leq R/2) \leq \epsilon/16$ , where  $R = \bar{R}(eK^{-1/12})$ , and let the step size  $\eta$  be  $\tilde{O}(\min\{\rho^2d^{-2}, B^2\rho^2d^{-4}\})$ . Under these conditions, the distribution of the K-th iteration in the SGLD process satisfies:

$$\|\mu_K^{\text{SGLD}} - p(\boldsymbol{\theta}, \boldsymbol{w} \mid \mathcal{D}_{\text{ft}}, \mathcal{D}_{\text{safe}})\|_{\text{TV}} \le \lambda (1 - C_0 \eta)^K + B^{-1} C_1 \eta^{1/2} + C_2 \eta^{1/2} + \epsilon/2,$$
 (20)

for some problem-dependent constant  $\lambda > 0$ ,  $C_0 = \tilde{O}(\rho^2)$ ,  $C_1 = \tilde{O}(R\rho^{-1})$ ,  $C_2 = \tilde{O}(d\rho^{-1})$ . Here  $\|\cdot\|_{\mathrm{TV}}$  stands for the total variation distance, and R is defined as:

$$\bar{R}(z) = \max \left\{ \frac{625d \log(4/z)}{m}, \quad \frac{4d \log(4L/m)}{m} + 4b, \quad \frac{4d + 8\sqrt{d \log(1/z)} + 8\log(1/z)}{m^{1/2}} \right\}. \tag{21}$$

# **H** Derivation of Equations

## H.1 Derivation of Eq. (1)

*Proof.* The decomposition of posterior distribution is primarily based on Bayes' theorem. The proof is presented below.

$$\begin{split} &p\left(\boldsymbol{\theta}, \boldsymbol{w} \mid \mathcal{D}_{\mathrm{ft}}, \mathcal{D}_{\mathrm{safe}}\right) \\ &= \frac{p\left(\boldsymbol{\theta}, \boldsymbol{w}, \mathcal{D}_{\mathrm{safe}} \mid \mathcal{D}_{\mathrm{ft}}\right)}{p\left(\mathcal{D}_{\mathrm{safe}} \mid \mathcal{D}_{\mathrm{ft}}\right)} \\ &= \underbrace{\frac{1}{p\left(\mathcal{D}_{\mathrm{safe}} \mid \mathcal{D}_{\mathrm{ft}}\right)}} \cdot p\left(\boldsymbol{\theta}, \mathcal{D}_{\mathrm{safe}} \mid \boldsymbol{w}, \mathcal{D}_{\mathrm{ft}}\right) \cdot p(\boldsymbol{w}) \\ &= \underbrace{\Delta \cdot p\left(\mathcal{D}_{\mathrm{safe}} \mid \boldsymbol{\theta}, \boldsymbol{w}, \mathcal{D}_{\mathrm{ft}}\right) \cdot p\left(\boldsymbol{\theta} \mid \boldsymbol{w}, \mathcal{D}_{\mathrm{ft}}\right) \cdot p(\boldsymbol{w})}_{= \Delta \cdot p\left(\mathcal{D}_{\mathrm{safe}} \mid \boldsymbol{\theta}\right) \cdot p\left(\boldsymbol{\theta} \mid \boldsymbol{w}, \mathcal{D}_{\mathrm{ft}}\right) \cdot p(\boldsymbol{w}) \\ &= \Delta \cdot p\left(\mathcal{D}_{\mathrm{safe}} \mid \boldsymbol{\theta}\right) \cdot \frac{p\left(\mathcal{D}_{\mathrm{ft}} \mid \boldsymbol{\theta}, \boldsymbol{w}\right) \cdot p\left(\boldsymbol{\theta} \mid \boldsymbol{w}\right)}{p\left(\mathcal{D}_{\mathrm{ft}} \mid \boldsymbol{w}\right)} \cdot p(\boldsymbol{w}) \\ &= \Delta \cdot p\left(\mathcal{D}_{\mathrm{safe}} \mid \boldsymbol{\theta}\right) \cdot p\left(\mathcal{D}_{\mathrm{ft}} \mid \boldsymbol{\theta}, \boldsymbol{w}\right) \cdot p\left(\mathcal{D}_{\mathrm{ft}} \mid \boldsymbol{w}\right)^{-1} \cdot p(\boldsymbol{\theta}, \boldsymbol{w}) \\ &\propto p(\mathcal{D}_{\mathrm{safe}} \mid \boldsymbol{\theta}) \cdot p(\mathcal{D}_{\mathrm{ft}} \mid \boldsymbol{\theta}, \boldsymbol{w}) \cdot p(\mathcal{D}_{\mathrm{ft}} \mid \boldsymbol{w})^{-1} \cdot p(\boldsymbol{\theta}, \boldsymbol{w}) \end{split}$$

#### H.2 Derivation of Eq. (4)

*Proof.* The complete proof is presented below.

$$\begin{split} & p\left(\mathcal{D}_{\mathrm{ft}} \mid \boldsymbol{w}\right)^{-1} \\ & \propto \left[ \int p\left(\mathcal{D}_{\mathrm{ft}} \mid \boldsymbol{\theta}, \boldsymbol{w}\right) \cdot p\left(\boldsymbol{\theta} \mid \boldsymbol{w}\right) \, \mathrm{d}\boldsymbol{\theta} \right]^{-1} \\ & \propto \left[ \int p\left(\mathcal{D}_{\mathrm{ft}} \mid \boldsymbol{\theta}, \boldsymbol{w}\right) \cdot \int p\left(\boldsymbol{\theta} \mid \mathcal{D}_{\mathrm{ft}}, \boldsymbol{w}\right) p\left(\mathcal{D}_{\mathrm{ft}} \mid \boldsymbol{w}\right) \, \mathrm{d}\mathcal{D}_{\mathrm{ft}} \, \mathrm{d}\boldsymbol{\theta} \right]^{-1} \\ & \propto \left[ \int p\left(\mathcal{D}_{\mathrm{ft}} \mid \boldsymbol{\theta}, \boldsymbol{w}\right) \cdot \mathbb{E}_{p\left(\mathcal{D}_{\mathrm{ft}} \mid \boldsymbol{w}\right)} \left[ p\left(\boldsymbol{\theta} \mid \mathcal{D}_{\mathrm{ft}}, \boldsymbol{w}\right) \right] \, \mathrm{d}\boldsymbol{\theta} \right]^{-1} \\ & \approx \left[ p\left(\mathcal{D}_{\mathrm{ft}} \mid \hat{\boldsymbol{\theta}}, \boldsymbol{w}\right) \right]^{-1} \propto \prod_{i=1}^{|\mathcal{D}_{\mathrm{ft}}|} \exp\left(\sigma(w_i) \cdot \ell\left(\boldsymbol{z}_i^{\mathrm{ft}}; \hat{\boldsymbol{\theta}}\right)\right) \\ & \text{s.t.,} \quad \hat{\boldsymbol{\theta}} = \arg\max_{\boldsymbol{\theta}} \mathbb{E}_{p\left(\mathcal{D}_{\mathrm{ft}} \mid \boldsymbol{w}\right)} \left[ \left( p\left(\boldsymbol{\theta} \mid \mathcal{D}_{\mathrm{ft}}, \boldsymbol{w}\right) \right) \right] \end{split}$$

#### H.3 Derivation of Eq. (10)

*Proof.* The complete proof is presented below.

$$\begin{split} &p\left(\boldsymbol{\theta},\boldsymbol{\phi}\mid\mathcal{D}_{\mathrm{ft}},\mathcal{D}_{\mathrm{safe}}\right)\\ &=\frac{p\left(\boldsymbol{\theta},\boldsymbol{\phi},\mathcal{D}_{\mathrm{safe}}\mid\mathcal{D}_{\mathrm{ft}}\right)}{p\left(\mathcal{D}_{\mathrm{safe}}\mid\mathcal{D}_{\mathrm{ft}}\right)}\\ &=\frac{1}{p\left(\mathcal{D}_{\mathrm{safe}}\mid\mathcal{D}_{\mathrm{ft}}\right)}\cdot p\left(\boldsymbol{\theta},\mathcal{D}_{\mathrm{safe}}\mid\boldsymbol{\phi},\mathcal{D}_{\mathrm{ft}}\right)\cdot p(\boldsymbol{\phi})\\ &=\underbrace{\frac{1}{p\left(\mathcal{D}_{\mathrm{safe}}\mid\mathcal{D}_{\mathrm{ft}}\right)}\cdot p\left(\boldsymbol{\theta},\mathcal{D}_{\mathrm{ft}}\right)\cdot p\left(\boldsymbol{\phi}\right)}_{:=\Delta_{1}}\cdot p\left(\mathcal{D}_{\mathrm{safe}}\mid\boldsymbol{\theta},\boldsymbol{\phi},\mathcal{D}_{\mathrm{ft}}\right)\cdot p\left(\boldsymbol{\theta}\mid\boldsymbol{\phi},\mathcal{D}_{\mathrm{ft}}\right)\cdot p(\boldsymbol{\phi})\\ &=\Delta_{1}\cdot p\left(\mathcal{D}_{\mathrm{safe}}\mid\boldsymbol{\theta}\right)\cdot p\left(\boldsymbol{\theta}\mid\boldsymbol{\phi},\mathcal{D}_{\mathrm{ft}}\right)\cdot p\left(\boldsymbol{w}\mid\boldsymbol{\phi},\mathcal{D}_{\mathrm{ft}}\right)\,\mathrm{d}\boldsymbol{w}\cdot p(\boldsymbol{\phi})\\ &=\Delta_{1}\cdot p\left(\mathcal{D}_{\mathrm{safe}}\mid\boldsymbol{\theta}\right)\cdot \int p\left(\boldsymbol{\theta}\mid\boldsymbol{w},\mathcal{D}_{\mathrm{ft}}\right)p\left(\boldsymbol{w}\mid\boldsymbol{\phi},\mathcal{D}_{\mathrm{ft}}\right)\,\mathrm{d}\boldsymbol{w}\cdot p(\boldsymbol{\phi})\\ &=\Delta_{1}\cdot p\left(\mathcal{D}_{\mathrm{safe}}\mid\boldsymbol{\theta}\right)\cdot p\left(\boldsymbol{\theta}\mid\boldsymbol{w}=\mathcal{N}(\mathcal{D}_{\mathrm{ft}};\boldsymbol{\phi}),\mathcal{D}_{\mathrm{ft}}\right)\cdot p(\boldsymbol{\phi})\\ &=\Delta_{1}\cdot p\left(\mathcal{D}_{\mathrm{safe}}\mid\boldsymbol{\theta}\right)\cdot \frac{p\left(\mathcal{D}_{\mathrm{ft}}\mid\boldsymbol{\theta},\boldsymbol{w}=\mathcal{N}(\mathcal{D}_{\mathrm{ft}};\boldsymbol{\phi})\right)}{p\left(\mathcal{D}_{\mathrm{ft}}\mid\boldsymbol{w}=\mathcal{N}(\mathcal{D}_{\mathrm{ft}};\boldsymbol{\phi})\right)}\cdot p\left(\boldsymbol{\theta}\mid\boldsymbol{w}=\mathcal{N}(\mathcal{D}_{\mathrm{ft}};\boldsymbol{\phi})\right)\cdot p(\boldsymbol{\phi})\\ &=\Delta_{1}\cdot p\left(\mathcal{D}_{\mathrm{safe}}\mid\boldsymbol{\theta}\right)\cdot \frac{p\left(\mathcal{D}_{\mathrm{ft}}\mid\boldsymbol{\theta},\boldsymbol{w}=\mathcal{N}(\mathcal{D}_{\mathrm{ft}};\boldsymbol{\phi})\right)}{p\left(\mathcal{D}_{\mathrm{ft}}\mid\boldsymbol{w}=\mathcal{N}(\mathcal{D}_{\mathrm{ft}};\boldsymbol{\phi})\right)}\cdot \int p(\boldsymbol{\theta}\mid\boldsymbol{w})\cdot p(\boldsymbol{w}\mid\boldsymbol{\phi},\mathcal{D}_{\mathrm{ft}})\,\mathrm{d}\boldsymbol{w}\cdot p(\boldsymbol{\phi})\\ &=\Delta_{1}\cdot p\left(\mathcal{D}_{\mathrm{safe}}\mid\boldsymbol{\theta}\right)\cdot \frac{p\left(\mathcal{D}_{\mathrm{ft}}\mid\boldsymbol{\theta},\boldsymbol{w}=\mathcal{N}(\mathcal{D}_{\mathrm{ft}};\boldsymbol{\phi})\right)}{p\left(\mathcal{D}_{\mathrm{ft}}\mid\boldsymbol{w}=\mathcal{N}(\mathcal{D}_{\mathrm{ft}};\boldsymbol{\phi})\right)}\cdot p(\boldsymbol{\theta}\mid\boldsymbol{\phi},\mathcal{D}_{\mathrm{ft}})\cdot p(\boldsymbol{\phi})\\ &=\Delta_{1}\cdot p\left(\mathcal{D}_{\mathrm{safe}}\mid\boldsymbol{\theta}\right)\cdot \frac{p\left(\mathcal{D}_{\mathrm{ft}}\mid\boldsymbol{\theta},\boldsymbol{w}=\mathcal{N}(\mathcal{D}_{\mathrm{ft}};\boldsymbol{\phi})\right)}{p\left(\mathcal{D}_{\mathrm{ft}}\mid\boldsymbol{w}=\mathcal{N}(\mathcal{D}_{\mathrm{ft}};\boldsymbol{\phi})\right)}\cdot p(\boldsymbol{\theta}\mid\boldsymbol{\phi},\mathcal{D}_{\mathrm{ft}})\cdot p(\boldsymbol{\phi})\\ &=\Delta_{1}\cdot p\left(\mathcal{D}_{\mathrm{safe}}\mid\boldsymbol{\theta}\right)\cdot \frac{p\left(\mathcal{D}_{\mathrm{ft}}\mid\boldsymbol{\theta},\boldsymbol{w}=\mathcal{N}(\mathcal{D}_{\mathrm{ft}};\boldsymbol{\phi})\right)}{p\left(\mathcal{D}_{\mathrm{ft}}\mid\boldsymbol{w}=\mathcal{N}(\mathcal{D}_{\mathrm{ft}};\boldsymbol{\phi})\right)}\cdot p(\boldsymbol{\theta}\mid\boldsymbol{\phi},\mathcal{D}_{\mathrm{ft}})\cdot p(\boldsymbol{\phi})\\ &=\Delta_{1}\cdot p\left(\mathcal{D}_{\mathrm{safe}}\mid\boldsymbol{\theta}\right)\cdot \frac{p\left(\mathcal{D}_{\mathrm{ft}}\mid\boldsymbol{\theta},\boldsymbol{w}=\mathcal{N}(\mathcal{D}_{\mathrm{ft}};\boldsymbol{\phi})\right)}{p\left(\mathcal{D}_{\mathrm{ft}}\mid\boldsymbol{\phi},\boldsymbol{w}=\mathcal{N}(\mathcal{D}_{\mathrm{ft}};\boldsymbol{\phi})\right)}\cdot p(\boldsymbol{\theta}\mid\boldsymbol{\phi},\mathcal{D}_{\mathrm{ft}})\cdot p(\boldsymbol{\phi})\\ &=\Delta_{1}\cdot p\left(\mathcal{D}_{\mathrm{safe}}\mid\boldsymbol{\theta}\right)\cdot \frac{p\left(\mathcal{D}_{\mathrm{ft}}\mid\boldsymbol{\theta},\boldsymbol{w}=\mathcal{N}(\mathcal{D}_{\mathrm{ft}};\boldsymbol{\phi})\right)}{p\left(\mathcal{D}_{\mathrm{ft}}\mid\boldsymbol{\phi},\boldsymbol{w}=\mathcal{N}(\mathcal{D}_{\mathrm{ft}};\boldsymbol{\phi})\right)}\cdot p(\boldsymbol{\theta}\mid\boldsymbol{\phi},\mathcal{D}_{\mathrm{ft}})\cdot p(\boldsymbol{\phi}\mid\boldsymbol{\phi},\boldsymbol{\phi}\mid\boldsymbol{\phi},\boldsymbol{\phi}\mid\boldsymbol{\phi})\\ &=\Delta_{1}\cdot p\left(\mathcal{D}_{\mathrm{safe}}\mid\boldsymbol{\phi$$

## H.4 Derivation of Eq. (16)

*Proof.* The softmax weight transformation is defined as follows:

$$\bar{\bar{\sigma}}(w_k) = \frac{e^{w_k}}{\sum_{i=1}^{|\mathcal{D}_{\text{ft}}|} e^{w_i}}, \quad k = 1, 2, \dots, |\mathcal{D}_{\text{ft}}|.$$

The partial derivative of  $\bar{\sigma}(w_k)$  with respect to  $w_i$  is given by

$$\frac{\partial \bar{\bar{\sigma}}(w_k)}{\partial w_i} = \begin{cases} \bar{\bar{\sigma}}(w_k) \cdot (1 - \bar{\bar{\sigma}}(w_k)), & \text{if } k = i\\ -\bar{\bar{\sigma}}(w_k) \cdot \bar{\bar{\sigma}}(w_i), & \text{if } k \neq i \end{cases}$$

From Eq. (8), the weight update rule is defined as:

$$oldsymbol{w} \leftarrow oldsymbol{w} + rac{\eta}{2} 
abla_{oldsymbol{w}} \left( \log p(oldsymbol{w}) - rac{|\mathcal{D}_{ ext{ft}}|}{|\mathcal{B}_{ ext{ft}}|} \sum_{oldsymbol{z}_k^{ ext{ft}} \in \mathcal{B}_{tr}} \left[ \bar{ar{\sigma}}\left(w_k\right) \cdot \ell\left(oldsymbol{z}_k^{ ext{ft}}
ight) 
ight] 
ight).$$

By taking the derivative of w and ignoring the prior term and constant coefficients, the gradient with respect to  $w_i$  is:

$$\frac{\partial}{\partial w_{i}} \left( \sum_{k=1}^{|\mathcal{D}_{\mathrm{ft}}|} \bar{\bar{\sigma}}\left(w_{k}\right) \cdot \ell\left(\boldsymbol{z}_{k}^{\mathrm{ft}}\right) \right) = \ell\left(\boldsymbol{z}_{i}^{\mathrm{ft}}\right) \cdot \bar{\bar{\sigma}}\left(w_{i}\right) \cdot \left(1 - \bar{\bar{\sigma}}\left(w_{i}\right)\right) - \sum_{k \neq i} \ell\left(\boldsymbol{z}_{k}^{\mathrm{ft}}\right) \cdot \bar{\bar{\sigma}}\left(w_{k}\right) \cdot \bar{\bar{\sigma}}\left(w_{i}\right).$$

Taking a further step, we can simplify it as:

$$\frac{\partial}{\partial w_{i}} \left( \sum_{k=1}^{|\mathcal{D}_{\mathrm{ft}}|} \bar{\bar{\sigma}}\left(w_{k}\right) \cdot \ell\left(\boldsymbol{z}_{k}^{\mathrm{ft}}\right) \right) = \bar{\bar{\sigma}}\left(w_{i}\right) \cdot \left(\ell\left(\boldsymbol{z}_{i}^{\mathrm{ft}}\right) - \sum_{k=1}^{|\mathcal{D}_{\mathrm{ft}}|} \bar{\bar{\sigma}}\left(w_{k}\right) \cdot \ell\left(\boldsymbol{z}_{k}^{\mathrm{ft}}\right) \right).$$

Using the derivative, the gradient update for  $w_i$  becomes:

$$abla_{w_i} = -ar{ar{\sigma}}\left(w_i
ight)\cdot\left(\ell\left(oldsymbol{z}_i^{ ext{ft}}
ight) - \sum_{k=1}^{|\mathcal{D}_{ ext{ft}}|}ar{ar{\sigma}}\left(w_k
ight)\cdot\ell\left(oldsymbol{z}_k^{ ext{ft}}
ight)
ight).$$

# I Concept of Posterior Bias

#### I.1 Motivation of Proposed Posterior Bias

**Motivation.** Directly sampling from  $p(\boldsymbol{w}, \boldsymbol{\theta} \mid \mathcal{D}_{\rm ft}, \mathcal{D}_{\rm safe})$  could introduce bias, as the weights  $\boldsymbol{w}$  might assign reduced importance to both the fine-tuning data and potentially harmful examples in  $\mathcal{D}_{\rm ft}$  to preserve the model's inherent safety alignment (see Fig. 5). As a result, while the model performs well on  $\mathcal{D}_{\rm safe}$ , it often struggles to generalize effectively to a held-out benign tuning dataset  $\mathcal{D}_{\rm ft}^{\rm val}$ , which serves as a test or validation set to evaluate fine-tuning performance. Ideally, sampling should be done from  $p(\boldsymbol{w}^*, \boldsymbol{\theta}^* \mid \mathcal{D}_{\rm ft}, \mathcal{D}_{\rm safe}, \mathcal{D}_{\rm ft}^{\rm val})$  so that  $\boldsymbol{w}^*$  can balance the trade-off between the model's performance on  $\mathcal{D}_{\rm safe}$  and  $\mathcal{D}_{\rm ft}^{\rm val}$  (i.e., trade off between safe alignment and fine-tuning objectives).

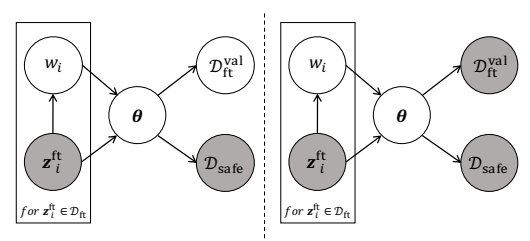


Illustration of posterior bias caused by the absence of  $\mathcal{D}_{\mathrm{ft}}^{\mathrm{val}}$ 

Figure 9: Illustration of posterior bias caused by the absence of  $\mathcal{D}_{\mathrm{ft}}^{\mathrm{val}}$ . Shaded nodes represent observed variables, while unshaded nodes denote unobserved variables.

# I.2 Definition of Posterior Bias

**Definition I.1.** (Posterior Bias) The posterior bias quantify the divergence, measured by a function  $D(\cdot)$ , between two posterior distributions: one derived solely from the alignment dataset  $\mathcal{D}_{safe}$  and the other incorporating a held-out clean tuning dataset  $\mathcal{D}_{ft}^{val}$ , which serves as a test or validation set to evaluate fine-tuning performance. Formally, it is defined as:

$$\mathcal{PB} = D(p(\mathbf{w}, \boldsymbol{\theta} \mid \mathcal{D}_{ft}, \mathcal{D}_{safe}) \mid p(\mathbf{w}^*, \boldsymbol{\theta}^* \mid \mathcal{D}_{ft}, \mathcal{D}_{safe}, \mathcal{D}_{ft}^{clean})).$$
(22)

Here, D refers to a divergence measure function between two distributions. Since attackers do not provide  $\mathcal{D}^{\mathrm{val}}_{\mathrm{ft}}$ , we can not directly derive an analytic formulation of Posterior Bias. By leveraging SGLD, we can derive an expression for the posterior bias by evaluating the expected difference in the T-th states of SGLD sampling trajectories. Next, we will introduce the definition of Empirical Posterior Bias with SGLD Sampling.

# I.3 Empirical Posterior Bias with SGLD Sampling

**Definition I.2.** (SGLD Sampling Trajectory) The SGLD Sampling Trajectory refers to the sequence of states during the iterative sampling process of SGLD. This sequence forms a Markov chain, where each state transition depends solely on the previous state. For the distribution  $p(\boldsymbol{w}, \boldsymbol{\theta} \mid \mathcal{D}_{\mathrm{ft}}, \mathcal{D}_{\mathrm{safe}})$ , the trajectories of the variables  $\boldsymbol{w}$  and  $\boldsymbol{\theta}$  can be defined as:

$$\operatorname{Tr}_{\boldsymbol{w}} = \boldsymbol{w}^{(0)} \to \cdots \to \boldsymbol{w}^{(T)}, \ \boldsymbol{w}^{(t+1)} = \boldsymbol{w}^{(t)} + \frac{\eta}{2} \nabla_{\boldsymbol{w}}^{(t)} + \epsilon \sqrt{\eta},$$

$$\operatorname{Tr}_{\boldsymbol{\theta}} = \boldsymbol{\theta}^{(0)} \to \cdots \to \boldsymbol{\theta}^{(T)}, \ \boldsymbol{\theta}^{(t+1)} = \boldsymbol{\theta}^{(t)} + \frac{\eta}{2} \nabla_{\boldsymbol{\theta}}^{(t)} + \epsilon \sqrt{\eta}.$$
(23)

Here, we use  $\nabla_{\boldsymbol{w}}$  and  $\nabla_{\boldsymbol{\theta}}$  to represent the gradient terms. Similarly, this definition can be extended to the distribution  $p\left(\boldsymbol{w}^*, \boldsymbol{\theta}^* \mid \mathcal{D}_{\mathrm{ft}}, \mathcal{D}_{\mathrm{safe}}, \mathcal{D}_{\mathrm{ft}}^{\mathrm{val}}\right)$ .

**Definition I.3.** (Empirical Posterior Bias with SGLD sampling) By leveraging SGLD sampling, posterior bias can be derived by evaluating the expected difference in the T-th states of the paired SGLD sampling trajectories  $\text{Tr}_{\boldsymbol{w}}$  and  $\text{Tr}_{\boldsymbol{w}^*}$  with identical initial states:

$$\mathcal{PB} = \underset{\text{Tr}_{\boldsymbol{w}}, \text{Tr}_{\boldsymbol{w}^*}}{\mathbb{E}} \left\| \boldsymbol{w}^{(T)} - \boldsymbol{w}^{*(T)} \right\| = \frac{\eta}{2} \cdot \underset{\text{Tr}_{\boldsymbol{w}}, \text{Tr}_{\boldsymbol{w}^*}}{\mathbb{E}} \sum_{t=0}^{T-1} \left\| \nabla_{\boldsymbol{w}}^{(t)} - \nabla_{\boldsymbol{w}^*}^{(t)} \right\|$$
$$= \frac{\eta}{2} \cdot \underset{\text{Tr}_{\boldsymbol{w}}, \text{Tr}_{\boldsymbol{w}^*}}{\mathbb{E}} \sum_{i=1}^{|\mathcal{D}_{\text{ft}}|} \sum_{t=0}^{T-1} \left\| \nabla_{w_i}^{(t)} - \nabla_{w_i^*}^{(t)} \right\|. \tag{24}$$

Here,  $\operatorname{Tr}_{\boldsymbol{w}}$  and  $\operatorname{Tr}_{\boldsymbol{w}^*}$  denote the SGLD sampling trajectories drawn from the target distributions  $p(\mathbf{w}, \boldsymbol{\theta} \mid \mathcal{D}_{\operatorname{ft}}, \mathcal{D}_{\operatorname{safe}})$  and  $p(\mathbf{w}^*, \boldsymbol{\theta}^* \mid \mathcal{D}_{\operatorname{ft}}, \mathcal{D}_{\operatorname{safe}}, \mathcal{D}_{\operatorname{ft}}^{\operatorname{clean}})$ , respectively. The norm used is the  $\ell_1$ -norm.

# I.4 Understanding Posterior Bias under Identity Weight Transformation

As shown in Eq. (24), the gradient term  $\nabla_w$  at each state contributes directly to the posterior bias. Here, we consider the identity weight transformation, which is defined as follows:

$$\sigma(w_i) = w_i. \tag{25}$$

Under identity weight transformation, the weight w updates in a monotonically decreasing manner:

$$\begin{cases}
\underbrace{-\ell\left(\boldsymbol{z}_{i}^{\mathrm{ft}};\boldsymbol{\theta}\right)}_{\nabla_{w_{i}}} \ll \underbrace{-\ell\left(\boldsymbol{z}_{i}^{\mathrm{ft}};\boldsymbol{\theta}^{*}\right)}_{\nabla_{w_{i}^{*}}} \approx 0, \text{ if } \boldsymbol{z}_{i}^{\mathrm{ft}} \in \mathcal{D}_{\mathrm{ft}}^{\mathrm{benign}} \\
\underbrace{-\ell\left(\boldsymbol{z}_{j}^{\mathrm{ft}};\boldsymbol{\theta}\right)}_{\nabla_{w_{j}}} \approx \underbrace{-\ell\left(\boldsymbol{z}_{j}^{\mathrm{ft}};\boldsymbol{\theta}^{*}\right)}_{\nabla_{w_{i}^{*}}} \ll 0, \text{ if } \boldsymbol{z}_{j}^{\mathrm{ft}} \in \mathcal{D}_{\mathrm{ft}}^{\mathrm{harmful}}
\end{cases} \tag{26}$$

The posterior bias under identity weight transformation arises mainly from updates in benign tuning data  $\boldsymbol{z}_i^{\mathrm{ft}} \in \mathcal{D}_{\mathrm{ft}}^{\mathrm{benign}}$ . Here,  $\boldsymbol{\theta}^* \sim p(\boldsymbol{\theta}^* \mid \mathcal{D}_{\mathrm{ft}}, \mathcal{D}_{\mathrm{safe}}, \mathcal{D}_{\mathrm{ft}}^{\mathrm{val}})$  fits an additional dataset  $\mathcal{D}_{\mathrm{ft}}^{\mathrm{val}}$ , while  $\boldsymbol{\theta} \sim p(\boldsymbol{\theta} \mid \mathcal{D}_{\mathrm{ft}}, \mathcal{D}_{\mathrm{safe}})$  does not. As a result,  $\boldsymbol{\theta}^*$  achieves a much lower loss on benign data, such that  $-\ell\left(\boldsymbol{z}_i^{\mathrm{ft}}; \boldsymbol{\theta}\right) \ll -\ell\left(\boldsymbol{z}_i^{\mathrm{ft}}; \boldsymbol{\theta}^*\right)$ . Since the gradient of  $\boldsymbol{w}$  is proportional to the negative loss, this results in a large and monotonically decreasing reduction in the weights for benign data, leading to poor fine-tuning performance. For harmful data  $\boldsymbol{z}_j^{\mathrm{ft}} \in \mathcal{D}_{\mathrm{ft}}^{\mathrm{harmful}}$ , which has different distribution from both  $\mathcal{D}_{\mathrm{ft}}^{\mathrm{benign}}$  and  $\mathcal{D}_{\mathrm{ft}}^{\mathrm{val}}$ , the loss remains high and the weights also monotonically decrease.

## I.5 Theorem of Time-Weighted Accumulation of Posterior Bias

While BDS demonstrates superior defensive performance, a theoretical understanding of the inherent suboptimality in inferred data weights offers deeper insights that can guide future algorithmic improvements. Here, we further explore weight suboptimality under identity transformation through the theoretical perspective of posterior bias:

**Theorem I.4** (Time-Weighted Accumulation of Posterior Bias, identical to Theorem 4.2 in the main paper). Let  $(\operatorname{Tr}_{\boldsymbol{w}}, \operatorname{Tr}_{\boldsymbol{\theta}})$  and  $(\operatorname{Tr}_{\boldsymbol{w}^*}, \operatorname{Tr}_{\boldsymbol{\theta}^*})$  denote the Stochastic Gradient Langevin Dynamics (SGLD) sampling trajectories drawn from the target distributions  $p(\boldsymbol{w}, \boldsymbol{\theta} \mid \mathcal{D}_{\mathrm{ft}}, \mathcal{D}_{\mathrm{safe}})$  and  $p(\boldsymbol{w}^*, \boldsymbol{\theta}^* \mid \mathcal{D}_{\mathrm{ft}}, \mathcal{D}_{\mathrm{safe}}, \mathcal{D}_{\mathrm{ft}}^{\mathrm{val}})$ , respectively. Here,  $\mathcal{D}_{\mathrm{ft}}^{\mathrm{val}}$  is a held-out clean tuning dataset, serving as a test or validation set to evaluate fine-tuning performance. Then, the following proportionality holds:

$$\underbrace{\mathbb{E}_{\mathbf{Tr}_{\boldsymbol{w}},\mathbf{Tr}_{\boldsymbol{w}^*}} \left\| \boldsymbol{w}^{(T)} - \boldsymbol{w}^{*(T)} \right\|}_{\mathcal{PB}^{(T)}} \propto \underbrace{\mathbb{E}_{\mathbf{Tr}_{\bar{\boldsymbol{w}}},\mathbf{Tr}_{\bar{\boldsymbol{w}}^*}} \sum_{t=0}^{T-1} (T-t) \left\| \boldsymbol{w}^{(t)} - \boldsymbol{w}^{*(t)} \right\|}_{\sum_{t=1}^{T-1} (T-t)\mathcal{PB}^{(t)}}.$$
(27)

Here,  $\mathbf{w}^{(T)}$  and  $\mathbf{w}^{*(T)}$  represent the sampled weights at iteration T, while  $\bar{\mathbf{w}}^{(t)}$  and  $\bar{\mathbf{w}}^{*(t)}$  denote the intermediate states of the trajectories at iteration t. The term  $\mathcal{PB}^{(T)}$  quantifies the posterior bias at the iteration T, and the summation  $\sum_{t=1}^{T-1} (T-t)\mathcal{PB}^{(t)}$  characterizes the cumulative posterior bias over the entire sampling trajectory.

**Implication.** Notably, the time-weighted factor T-t emphasizes the greater influence of earlier iterations on the cumulative bias, highlighting the cumulative effect of initial steps on the posterior inference. This suggests that suboptimal sampling in the early stages of SGLD sampling trajectory can propagate and aggressively affect the overall posterior inference. Future work could focus on developing bias management strategies, particularly for mitigating bias in early stages of SGLD sampling trategories.

#### I.6 Proof of theorem Theorem 4.2

*Proof.* Based on Definition I.3, the calculation formula for the SGLD-based posterior bias at T iteration is given as follows:

$$\begin{split} \mathcal{P}\mathcal{B}^{(T)} &= \underset{\mathsf{Tr}_{\boldsymbol{w}},\mathsf{Tr}_{\boldsymbol{w}^*}}{\mathbb{E}} \left\| \boldsymbol{w}^{(T)} - \boldsymbol{w}^{*(T)} \right\| \\ &= \frac{\eta}{2} \cdot \underset{\mathsf{Tr}_{\boldsymbol{w}},\mathsf{Tr}_{\boldsymbol{w}^*}}{\mathbb{E}} \sum_{t=0}^{T-1} \left\| \nabla_{\boldsymbol{w}}^{(t)} - \nabla_{\boldsymbol{w}^*}^{(t)} \right\| = \frac{\eta}{2} \cdot \underset{\mathsf{Tr}_{\boldsymbol{w}},\mathsf{Tr}_{\boldsymbol{w}^*}}{\mathbb{E}} \sum_{i=1}^{|\mathcal{D}_{\mathrm{ft}}|} \sum_{t=0}^{T-1} \left\| \nabla_{w_i}^{(t)} - \nabla_{w_i^*}^{(t)} \right\|. \end{split}$$

The SGLD sampling trajectory for w drawn from  $p(w, \theta \mid \mathcal{D}_{\text{ft}}, \mathcal{D}_{\text{safe}})$  is expressed as:

$$\operatorname{Tr}_{\boldsymbol{w}} = \boldsymbol{w}^{(0)} \to \cdots \to \boldsymbol{w}^{(T)}, \quad \boldsymbol{w}^{(t)} = \boldsymbol{w}^{(t)} + \frac{\eta}{2} \nabla_{\boldsymbol{w}}^{(t+1)} + \epsilon \sqrt{\eta},$$

$$\nabla_{w_i}^{(t)} = \nabla_{w_i} \log p(\boldsymbol{w}) - \ell(\boldsymbol{z}_i^{\mathrm{ft}}; \boldsymbol{\theta}^{(t)}).$$

Similarly, the SGLD sampling trajectory for  $\mathbf{w}^*$  drawn from  $p\left(\mathbf{w}^*, \mathbf{\theta}^* \mid \mathcal{D}_{\mathrm{ft}}, \mathcal{D}_{\mathrm{safe}}, \mathcal{D}_{\mathrm{ft}}^{\mathrm{val}}\right)$  is expressed as:

$$\mathrm{Tr}_{\boldsymbol{w}^*} = \boldsymbol{w}^{*(0)} \to \cdots \to \boldsymbol{w}^{*(T)}, \quad \boldsymbol{w}^{*(t+1)} = \boldsymbol{w}^{(t)} + \frac{\eta}{2} \nabla_{\boldsymbol{w}^*}^{(t)} + \epsilon \sqrt{\eta}$$

$$\nabla_{w_i^*}^{(t)} = \nabla_{w_i^*} \log p(\boldsymbol{w}) - \ell(\boldsymbol{z}_i^{\text{ft}}; \boldsymbol{\theta}^{*(t)}).$$

Similarly, the SGLD sampling trajectory of  $\theta$  drawn from  $p(w, \theta \mid \mathcal{D}_{\text{ft}}, \mathcal{D}_{\text{safe}})$  is expressed as:

$$\operatorname{Tr}_{\boldsymbol{\theta}} = \boldsymbol{\theta}^{(0)} \to \cdots \to \boldsymbol{\theta}^{(T)}, \quad \boldsymbol{\theta}^{(t+1)} = \boldsymbol{\theta}^{(t)} + \frac{\eta}{2} \nabla_{\boldsymbol{\theta}}^{(t)} + \epsilon \sqrt{\eta},$$

$$\nabla_{\boldsymbol{\theta}}^{(t)} = \nabla_{\boldsymbol{\theta}} \log p(\boldsymbol{\theta}) - \sum_{i=1}^{|\mathcal{D}_{\text{ft}}|} w_i^{(t)} \nabla_{\boldsymbol{\theta}} l\left(\boldsymbol{z}_i^{\text{ft}}; \boldsymbol{\theta}^{(t)}\right).$$

Similarly, the SGLD sampling trajectory of  $\theta^*$  drawn from  $p\left(w^*, \theta^* \mid \mathcal{D}_{\mathrm{ft}}, \mathcal{D}_{\mathrm{safe}}, \mathcal{D}_{\mathrm{ft}}^{\mathrm{val}}\right)$  is expressed as:

$$\mathrm{Tr}_{\boldsymbol{\theta}^*} = \boldsymbol{\theta}^{*(0)} \to \cdots \to \boldsymbol{\theta}^{*(T)}, \quad \boldsymbol{\theta}^{*(t+1)} = \boldsymbol{\theta}^{*(t)} + \frac{\eta}{2} \nabla_{\boldsymbol{\theta}}^{*(t)} + \epsilon \sqrt{\eta},$$

$$\nabla_{\boldsymbol{\theta}^*}^{(t)} = \nabla_{\boldsymbol{\theta}^*} \log p(\boldsymbol{\theta}^*) - \sum_{i=1}^{|\mathcal{D}_{\mathrm{ft}}|} w_i^{*(t)} \nabla_{\boldsymbol{\theta}^*} l\left(\boldsymbol{z}_i^{\mathrm{ft}}; \boldsymbol{\theta}^{*(t)}\right) - \sum_{i=1}^{|\mathcal{D}_{\mathrm{safe}}|} \nabla_{\boldsymbol{\theta}^*} l\left(\boldsymbol{z}_j^{\mathrm{safe}}; \boldsymbol{\theta}^{*(t)}\right).$$

Under the identity transformation, we compute the gradient difference for  $w_i$  at the t-th iteration as follows:

$$||\nabla_{w_i}^{(t)} - \nabla_{w_i^*}^{(t)}|| = ||\ell(\mathbf{z}_i^{\text{ft}}; \boldsymbol{\theta}^{*(t)}) - \ell(\mathbf{z}_i^{\text{ft}}; \boldsymbol{\theta}^{(t)})|| = ||\Delta \ell_i^{(t)}||.$$

Here, the difference in loss is approximated using the Taylor expansion, yielding:

$$\begin{split} ||\Delta\ell_{i}^{(t)}|| &= ||\ell(\boldsymbol{z}_{i}^{\mathrm{ft}};\boldsymbol{\theta}^{*(t)}) - \ell(\boldsymbol{z}_{i}^{\mathrm{ft}};\boldsymbol{\theta}^{(t)})|| \approx \left\| \nabla_{\boldsymbol{\theta}} \ell\left(\boldsymbol{z}_{i}^{\mathrm{ft}};\boldsymbol{\theta}^{(t)}\right)^{\top} \left(\boldsymbol{\theta}^{*(t)} - \boldsymbol{\theta}^{(t)}\right) \right\| \\ &= \frac{\eta}{2} \cdot \sum_{k=0}^{t-1} \left\| \frac{\nabla_{\boldsymbol{\theta}} \ell\left(\boldsymbol{z}_{i}^{\mathrm{ft}};\boldsymbol{\theta}^{(t)}\right)^{\top} \left(\nabla_{\boldsymbol{\theta}^{*}}^{(k)} - \nabla_{\boldsymbol{\theta}^{(k)}}^{(k)}\right) \right\| \\ &= \frac{\eta}{2} \cdot \sum_{k=0}^{t-1} \left\| \nabla_{\boldsymbol{\theta}} \ell^{\top} \left( \sum_{i=1}^{|\mathcal{D}_{\mathrm{f}}|} \left(w_{i}^{*(k)} - w_{i}^{(k)}\right) \nabla_{\boldsymbol{\theta}} \ell\left(\boldsymbol{z}_{i}^{\mathrm{ft}};\boldsymbol{\theta}^{(k)}\right) + \sum_{j=1}^{|\mathcal{D}_{\mathrm{safe}}|} \left[\nabla_{\boldsymbol{\theta}} \ell\left(\boldsymbol{z}_{j}^{\mathrm{safe}};\boldsymbol{\theta}^{(k)}\right) - \nabla_{\boldsymbol{\theta}} \ell\left(\boldsymbol{z}_{j}^{\mathrm{safe}};\boldsymbol{\theta}^{*(k)}\right) \right] \right) \right\| \\ &= \frac{\eta}{2} \cdot \sum_{k=0}^{t-1} \left\| \nabla_{\boldsymbol{\theta}} \ell^{\top} \left( \left(\boldsymbol{w}^{*(k)} - \boldsymbol{w}^{(k)}\right)^{\top} \nabla_{\boldsymbol{\theta}} \ell\left(\mathcal{D}^{\mathrm{ft}};\boldsymbol{\theta}^{(k)}\right) + \sum_{j=1}^{|\mathcal{D}_{\mathrm{safe}}|} \left[\nabla_{\boldsymbol{\theta}} \ell\left(\boldsymbol{z}_{j}^{\mathrm{safe}};\boldsymbol{\theta}^{(k)}\right) - \nabla_{\boldsymbol{\theta}} \ell\left(\boldsymbol{z}_{j}^{\mathrm{safe}};\boldsymbol{\theta}^{*(k)}\right) \right] \right) \right\| \\ &\approx \frac{\eta}{2} \cdot \sum_{k=0}^{t-1} \left\| \nabla_{\boldsymbol{\theta}} \ell\left(\boldsymbol{z}_{i}^{\mathrm{f}};\boldsymbol{\theta}^{(t)}\right)^{\top} \left( \left(\boldsymbol{w}^{*(k)} - \boldsymbol{w}^{(k)}\right)^{\top} \nabla_{\boldsymbol{\theta}^{(k)}} \ell\left(\mathcal{D}^{\mathrm{ft}};\boldsymbol{\theta}^{(k)}\right) \right) \right\| \\ &\propto \frac{\eta}{2} \cdot \sum_{k=0}^{t-1} \left\| \nabla_{\boldsymbol{\theta}} \ell\left(\boldsymbol{z}_{i}^{\mathrm{ft}};\boldsymbol{\theta}^{(t)}\right) \right\| \cdot \left\| \boldsymbol{w}^{*(k)} - \boldsymbol{w}^{(k)} \right\| \cdot \left\| \nabla_{\boldsymbol{\theta}^{(k)}} \ell\left(\mathcal{D}^{\mathrm{ft}};\boldsymbol{\theta}^{(k)}\right) \right\| . \end{split}$$

The gradient term is calculated as follows:

$$abla_{m{ heta}} \ell\left(\mathcal{D}^{ ext{ft}}; m{ heta}^{(k)}
ight) = \left[egin{array}{c} 
abla_{m{ heta}^{(k)}} l\left(m{z}_1^{ ext{ft}}; m{ heta}^{(k)}
ight) \\ 
abla_{m{ heta}^{(k)}} l\left(m{z}_2^{ ext{ft}}; m{ heta}^{(k)}
ight) \\ 
& dots \\ 
abla_{m{ heta}^{(k)}} l\left(m{z}_{1}^{ ext{ft}}; m{ heta}^{(k)}
ight) 
onumber \end{array}
ight]$$

The gradient difference is proportional to the cumulative weight difference over previous steps:

$$\|\nabla_{w_i}^{(t)} - \nabla_{w_i^*}^{(t)}\| \propto \sum_{k=0}^{t-1} \|\boldsymbol{w}^{*(k)} - \boldsymbol{w}^{(k)}\|.$$

We substitute this into the definition of  $\mathcal{PB}^{(T)}$ :

$$\mathcal{PB}^{(T)} \propto \mathbb{E} \sum_{t=0}^{T-1} \sum_{k=0}^{t-1} \| oldsymbol{w}^{*(k)} - oldsymbol{w}^{(k)} \|.$$

Rearrange the double summation by swapping the summation order:

$$\sum_{t=0}^{T-1} \sum_{k=0}^{t-1} = \sum_{k=0}^{T-1} \sum_{t=k+1}^{T}.$$

Substitute this back into the equation:

$$\mathcal{PB}^{(T)} \propto \mathbb{E} \sum_{k=0}^{T-1} (T-k) \| \boldsymbol{w}^{*(k)} - \boldsymbol{w}^{(k)} \|,$$

where (T - k) represents the remaining time steps from step k to T.

Transforming this with the expression of  $\mathcal{PB}^{(t)}$ , we obtain:

$$\mathcal{PB}^{(T)} \propto \sum_{t=0}^{T-1} (T-t) \mathcal{PB}^{(t)}.$$